People's Democratic Republic of Algeria Ministry of Higher Education and Scientific Research

Echahid Hamma Lakhdar University of El-Oued

FACULTY OF TECHNOLOGY

MECHANICAL ENGINEERING DEPARTMENT

End of study thesis
Presented for the graduation of
ACADEMIC MASTER

Field: Technologies
Sector: Mechanical engineering
Specialty: Renewable Energies

Theme:

Exploitation and use of solar energy to Synthesis and characterization of Pure and Cobalt-doped NiO Nanoparticles by spray pyrolysis

In front of the jury composed of:

Dr.Meneceur Redha	President
Dr.Hamdi Omar	Examiner
Dr. Aoun Yacine	Supervisor

Presented by:

- Sadani Younes
- Slimani Soufiane
- Kouidi Tarek

2019-2020

ACKNOWLEDGEMENT:

We thank, first of all, Allah the Almighty for giving us the will and patience to carry out this modest work.

I would like to express my special thanks of gratitude to our supervisor AOUN.Y

Which also helped us in doing a lot of Research and we came to know about so many new things we are really thankful to them.

Also we deliver a special word of appreciation and gratitude to the examining committee for having the time and devotion to evaluate oue modest work

Secondly we would also like to thank our parents and friends who helped us a lot in finalizing this project within the limited time frame.

DEDICATION

This modest work is dedicated:

To our parents:

Thanks to their tender encouragement and great sacrifices, they were able to create the climate of affection and

conducive to the pursuit of our studies.

No dedication could express our respects, our considerations and our deep feelings towards them.

We pray to the good Lord to bless them, to watch over them, hoping that they will always be proud of us.

To our brothers.

To all our teachers:

Their generosity and support obliges me to show them our deep respect and our loyal consideration.

To all our friends and colleagues

And to all those who have contributed from near or far to make this project possible,

We Say thank you.

Contents

Contents

LIST OF FIGURES:

Chapter I: General information on solar energy

Chapter II: Thin films NiO-Co and deposition techniques

LIST OF TABLES:

NOMENCLATURE:

RATING UNITS

PVD: Physical Vapor Deposition

CVD: Chemical Vapor Deposition

$APCVD$: Atmospheric Pressure Chemical Vapor Deposition

$MOCVD$: Metal-Organic Chemical Vapor Deposition

$PECVD$: Plasma Enhanced Chemical Vapor Deposition

MBE: Molecular Beam Epitaxy

$LPCVD$: Low- Pressure Chemical Vapor Deposition

eHP: Half height of the heating plate (heating wire placed in the center) $[m]$

THP: Temperature of the heating wire $[°\,c]$

$esubstrate$: Height of the substrate $[m]$

T_{12}: Temperature at the plate / substrate interface $[°\,c\,]$

$T_{substrat}$: Temperature at the surface of the substrate $[°\,c]$

T_0: Temperature of the ambient medium $[°\,c]$

$\varphi_{cond\,1}$: Density of conduction flux in the heating plate

$\varphi_{cond\,2}$: Density of conduction flux in the substrate

$\emptyset_{conv}$: Density of convection flow between the ambient medium and the surface of the substrate

TCO: Transparent Conductive Oxides

CDO: Conductive Cadmium Oxide

σ: Electrical conductivity $[\mho^{-1}.cm^{-1}]$

μ: Mobility	$[\frac{Cm^2}{V.S}]$
N: Electronic densities	$[cm^3]$
E_g: Band gap energy (optical gap)	$[eV]$
ε: Dielectric constant	$[F\ /\ m]$
LCD: Liquid Crystal Display	
d_{hkl}: Inter-reticular distance	[Å]
a: mesh parameter	[Å]
θ: Angle of incidence (angle of reflection)	$[degree]$
λ: Wavelength of incident X photons	[Å]
n: Diffraction order (whole number)	
D: Size of crystallites	$[nm]$
β: Width at mid-height of the diffraction line	$[degree]$
α: Absorption coefficient	
h: Planck constant or 6,63.10^{-34}	$[J.s]$
v: Wave frequency	$[Hz]$
λ_{Eg}: Wavelength corresponding to the optical gap (Eg)	[Å]
E_U: Urbach energy	$[J]$
R_s: Surface resistance	$[\Omega]$
ρ: Electrical resistivity	$[\Omega.cm]$
I: Current intensity	$[A]$
U: current voltage	$[V]$

ε: Average stress [%]

δ: dislocation density $[\frac{lines}{m^2}]$

T: transmittance [%]

t: the thickness $[nm]$

α: absorption coefficient $[m^{-1}]$

GENERAL INTRODUCTION

General Introduction

Transparent and conductive oxides (TCO) are remarkable materials in many areas. The existence of their double property, electrical conductivity and transparency in the visible, makes them ideal candidates for applications in optoelectronics, photovoltaics or Electrochromic windows.[1]

The TCO have other applications, such as optical sensors, transparent electrical contacts in solar cells, flat screens, liquid crystal displays and touch screens [2].

The use of thin films is particularly interesting in areas where miniaturization and low dimensionality of devices are indispensable, as in the microelectronics industry.[3]

Among these, materials, nickel oxides (NiO) received a lot of attention due to their good electrochemical stability and electrocatalytic activity as well as the low cost for extended applications, with potential applications in various technologies such as Li+ batteries, super capacitors, gas sensors, photocatalysts and Electrochromic materials. In addition, it has been reported that NiO is an interesting semiconductor for optoelectronic devices[1]

The objective of this memory work is to master the synthesis of nickel oxide films by the pyrolysis spray technique and to study the effect of cobalt doping on the structural, optical and electrical properties of these films.

After a brief introduction to this work, the first chapter is devoted to a bibliographical study on solar energy, the properties of the sun, then solar radiation and its composition and the solar deposit in Algeria, thus the heat transfer and the three transfer ways and the applications of solar energy.

The second chapter, first of all includes some different deposition processes which currently allow to obtain transparent conductive oxides thin films , then the general properties of NiO (crystallographic, optical and electrical) and its applications as well, Some properties of cobalt.

The third chapter, a detailed study on the development of thin films of nickel oxide with and without doping, deposited on glass substrates. A reminder on characterization techniques used in this work such as X-ray diffraction for microstructural characterization, UV-Visible

spectroscopy for optical characterization and the four-point technique for electrical measurements.

Finally, encompasses all the experimental results obtained and their interpretations on the development of thin films of nickel oxide with and without doping and their properties.

I Chapter I :

General information on solar energy

I.1 Introduction

The energy field is growing every year for this reason research is needed on another new energy source more precisely renewable energies and in particular solar energy. Solar energy is presented by two systems: Solar thermal system (heat) like solar thermal collectors and solar photovoltaic system (electricity) like solar photovoltaic collectors (solar panel).

In this work we will be interested in the thermal exploitation of solar energy using a parabolic solar collector.

I.2 Sun

The Sun is the star at the center of the Solar System. It is almost perfectly spherical and consists of hot plasma interwoven with magnetic fields. It has a diameter of about 1,392,000 km, about 109 times that Earth, and its mass accounts for about 99.86% of the total mass of the Solar System. Chemically, about three quarters of the Sun's mass consists of hydrogen, while the rest is mostly helium. Less than 2% consists of heavier elements, including oxygen, carbon, neon, iron, and others[4].

The Sun is the primary source of energy for the Earth because of the thermonuclear chain reactions that take place on its surface. Seen from the Earth, the Sun subtends an angle of 32´ in the sky **(Figure I.1)**.

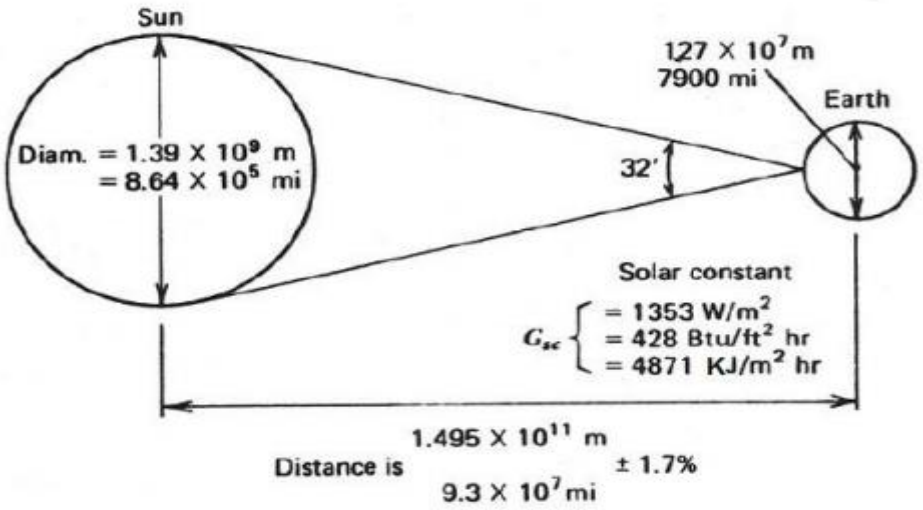

Figure I.1: *Sun - Earth relationships.*

Although considerable distance separates the earth and the sun yet the beneficial effects of the sun is felt greatly on earth. For example, sunlight is responsible for photosynthesis as well as vitamins D precursor synthesis yet its harmful effects after excessive exposure to ultraviolet rays of the sun have also been reported [4].

I.3 Solar radiation

The radiation or solar spectrum is comparable to that of a black body at a temperature of 5800 K, it is included in a band of wavelength varying from 0.22 to 10 μm and decomposes approximately on 3 bands:

- 9% in the Ultraviolet band (<0.4μm)

- 47% in the visible band (0.4 to 0.8μm)

- 44% in the infrared band (> 0.8μm)

The solar energy received on earth outside the atmosphere is estimated at 1370 W/m^2 however it attenuates and loses its intensity by crossing the atmosphere not exceeding 1000 W/m^2on the surface of the earth due of the absorption in the latter, this figure will subsequently vary depending on the geographic location of the site (latitude), the season, the time, the weather conditions (cloudiness, dust, humidity, etc.), and the altitude of the location.

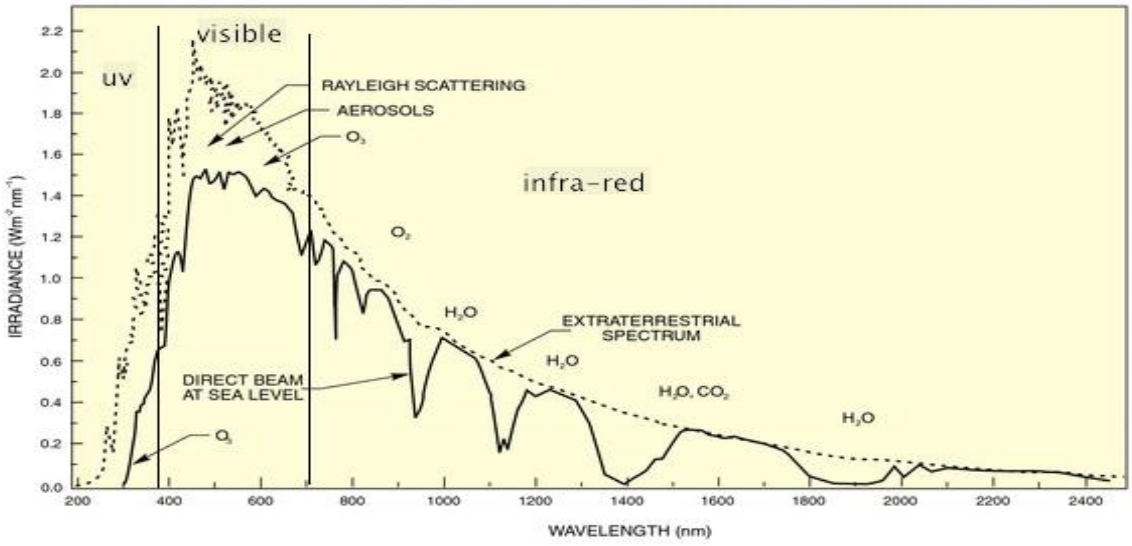

Figure I.2: *Spectrum of solar radiation*.

Being absorbed and diffused by crossing the atmosphere only a modified fraction of the solar radiation reaches the surface of the earth consisting of 3 different types of radiation:

- **Direct Radiation:** radiation received directly from the sun. It can be measured by a pyrheliometer.
- **Diffused Radiation**: radiation from the entire sky. This radiation is due to the absorption and diffusion of part of the solar radiation by the atmosphere and its reflection by the clouds. It can be measured by a pyranometer with a screen masking the sun.
- **Reflected Solar Radiation or the albedo of the ground:** the radiation which is reflected by the ground or by objects on its surface. This albedo can be important when the ground is particularly reflective (water, snow).
- **Overall Radiation:** the sum of all the radiation received, including the radiation reflected by the ground and the objects on its surface. It is measured by a pyranometer or a solarimeter without a screen.

Note that some solar collectors concentrate solar radiation in order to increase the efficiency of the collector compared to a given surface. These concentration sensors can only use direct radiation from the sun. In places with a high proportion of diffuse sunshine, these sensors cannot work effectively because the diffuse sunshine cannot be concentrated at one point.

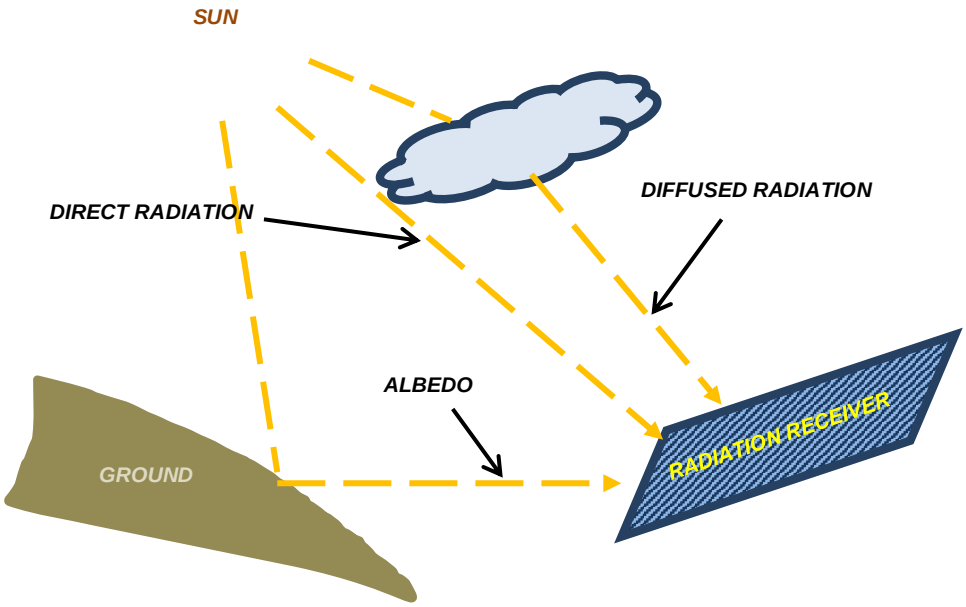

Figure I.3: *Different radiation components.*

I.4 The solar deposit in Algeria

The history of using solar energy in Algeria backs to 1954 with the solar furnace built by the French for ceramic fabrication purposes. Because of its geographic position, Algeria is considered one of the best places for solar energy usage. The insulation time over the quasi-totality of the national territory exceeds 2000 h annually and may reach 3900 h (high plains and Sahara). The daily obtained energy on a horizontal surface of $1m^2$ is of 5 kWh over the major part of the national territory, or about (1700 $k\,wh/m^2$/year) for the North and (2263 $k\,wh/m^2$/year) for the South of the country (**Table I.1 and Figure I.4**)[5].

Table.I.1: *Solar potential in Algeria.*

Areas	Costa area	Hight plateau	Sahara
Surface (%)	4	10	86
Average duration of sunning (h/ year)	2650	3000	3500
Received average energy(kwh/$\mathbf{m^2}$/year)	1700	1900	2650

In a large scale, the HassiR'Mel hybrid power plant is the first gas-solar power plant in Algeria; it is located in the region Tilghemt, 25 km north of HassiR'Mel largest gas field in Africa. It started in July2011, with a capacity of 150 megawatts (MW), the power plant will combine an array of parabolic trough concentrating solar power of 30 (MW), in an area of 180,000 m^2 and in conjunction with a gas turbine power plant of 120 megawatts, and the power plant is connected to the national electricity grid. It will have a positive impact on the environment and will reduce the amount of gas burned in favor of solar fields and also to reduce 33,000 tons of CO_2emissions. Also an amount of 7 million cubic meters of gas will be saved. With a total cost of 350 million euros, the central HassiR'Mel was conducted under a partnership agreement signed in 2006 between the Algerian society NEAL (New Energy Algeria) and the Spanish company Abengoa. The start of this plant is an important step in the promotion and use of solar thermal energy as program of electrical energy. It also marks the effective start of

implementation of the National Renewable Energy program adopted by the government in February 2011. This plant justifies further implementation in HassiR'Mel like the division dedicated to training and research in the field of renewable energy particularly in solar energy. Other plants were already scheduled; two stations.

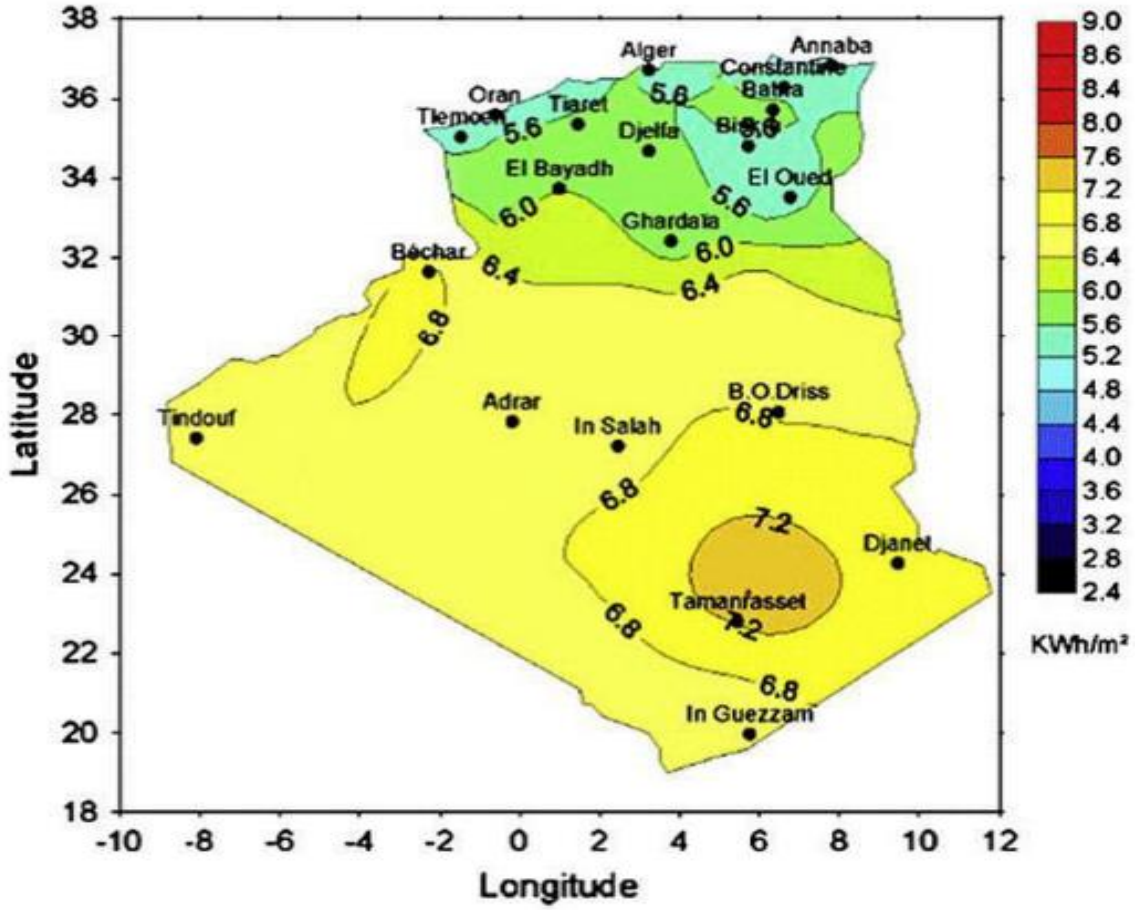

Figure I.4: *The Algerian solar map*[5].

On the same principle are scheduled for 2013, in eastern Algeria, the solar power plant Maghaïr in the state of El-Oued and to the west the solar power plant Naama in the state of El-Bayad. In Algeria, we must realize the maximum possible SEGS for more than possible reason beside environmental aspect; Algeria is considered the best region close to Europe to generate clean power to supply human kind with enough electricity on a sustainable basis like in the DESERTEC project (**FigureI.5)**.

Here comes the importance of doing such researches, like the Algerian Solar One HassiR'Mel (**FigureI.6**.)

Figure I.5: *DESERTEC Project.*

Figure I.6: *Solar Field Of HassiR'Mel Hybrid Power Plant.*

I.5 Solar energy

Solar energy is the radiation from the Sun capable of producing heat, causing chemical reactions or producing electricity, these solar rays are made up of photons, which reach us as energy carriers. This term solar energy is meant today solar electricity and thermal energy obtained from the exploitation of the sun in photovoltaic and photo thermal forms[6].

I.6 Solar energy exploitation

Three families of solar energy transformation processes stand out today:

I.6.1 Solar Thermal:

Solar thermal energy consists in using the heat of solar radiation.

I.6.1.a Passive Solar Thermal*:*

As the name suggests, the operating techniques of this form of solar energy does not require any mechanical or electrical equipment. They happen passively. We can find some kinds of use of this energy in (**Figure I.7)**:

- ***The building****: s*heating represents almost 50% of the energy needs of homes and businesses. This use of solar radiation reduces this cost.
- ***Trombe wall:*** This heating principle uses the phenomenon of a greenhouse by heating a wall (thermal mass) protected by a glass surface. The heat transfer to the interior of the building is effected by the circulation of air passing through this wall towards the interior .

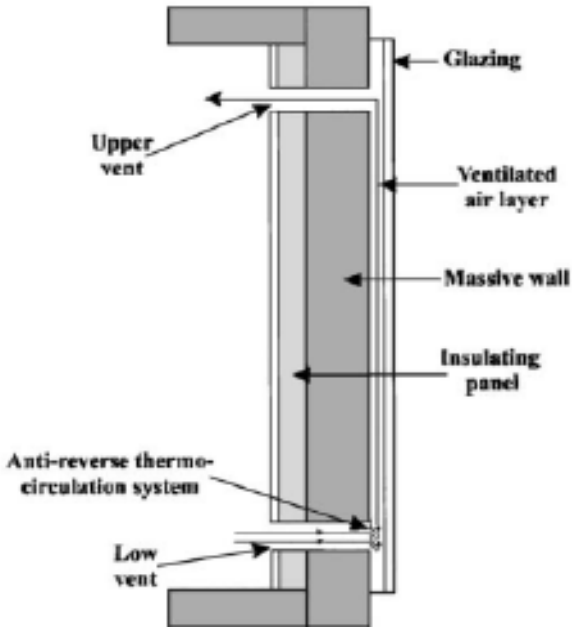

Figure I.7: *Examples of passive solar thermal.*

I.6.1.b *Active Solar Thermal:*

Active solar technology serves to capture the thermal energy of the solar radiation to transmit it to a heat transfer fluid which makes transport the thermal energy either to heat buildings or to generate domestic hot water**(Figure I.8)** [7].

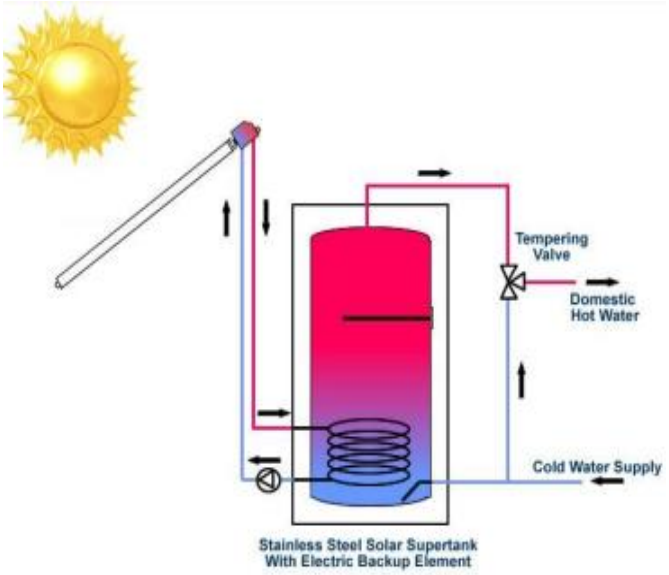

Figure I.8: *Domestic hot water system*[7].

I.6.2 Photovoltaic Solar (PV):

Photovoltaic (PV) is a method of generating electrical energy by converting solar radiation into direct current electricity using semiconductors that exhibit the photovoltaic effect. Photovoltaic electricity production uses **(Figure I.9)**:

- **PV Modules:** to convert sunlight instantly into DC electric power.
- **Inverter:** to convert DC power into standard AC power for home use
- **Battery:** to store the energy produced by the panels in the event of excess and to redistribute it in the event of demand.
- **Transformer:** to change the voltage in the installation for being able to connect with the distribution network. It is used a low voltage – medium voltage transformer.
- **Charge Controller:** to prevent battery overcharging and to prolong the battery life of your PV system.

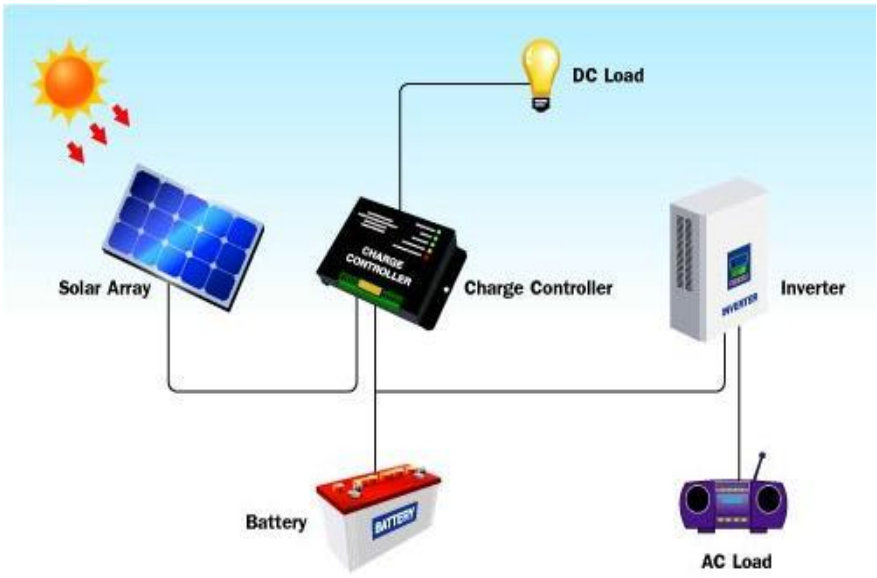

Figure I.9: *Photovoltaic solar system.*

I.6.3 Thermodynamic Solar (CSP):

Solar thermodynamics is a technique used to generate electricity or to benefit from high temperature. Photovoltaic conversion converts solar radiation directly into electricity, thermodynamic solar converts it into heat and then involves an electrical conversion device. The latter is known as CSP (Concentrated Solar Power), transforms the energy of solar radiation into heat, then converts this heat into mechanical and electrical energy using a thermodynamic cycle engine coupled to an electric generator. (For example a turbine and a generator). Thermodynamic solar energy is effective in countries with strong sunshine such as Algeria.

Among the techniques used in this type we find:

I.6.3.a Parabolic trough collectors (PTC) *:*

Consisting of parallel rows of long cylindro-parabolic mirrors (See **Figure I.10**) rotate around a horizontal axis to track solar radiation. The latter is concentrated on a horizontal receptor tube in which a heat transfer medium with a temperature of generally 400°C circulates. This fluid is then pumped through heat exchangers to produce superheated steam that drives a turbine or an electrical generator[8].

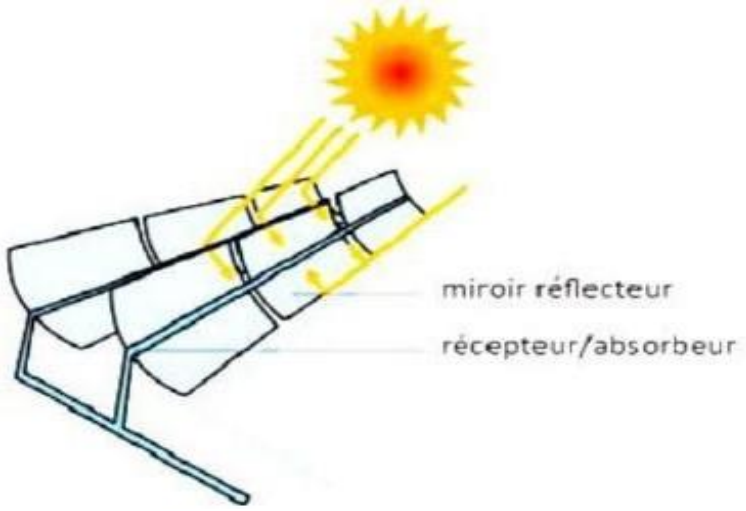

Figure I.10: *Parabolic trough collectors.*

I.6.3.b Heliostat field collector (HFC)

It can be used for extremely high inputs of radiant energy to reflect their incident direct solar radiation onto a common target as shown in (**Figure I.11)**. This is called the heliostat field or central receiver collector. By using slightly concave mirror segments on the heliostats, large amounts of thermal energy can be directed into the cavity of a steam generator to produce steam at high temperature and pressure.

The concentrated heat energy absorbed by the receiver is transferred to a circulating fluid that can be stored and later used to produce power.

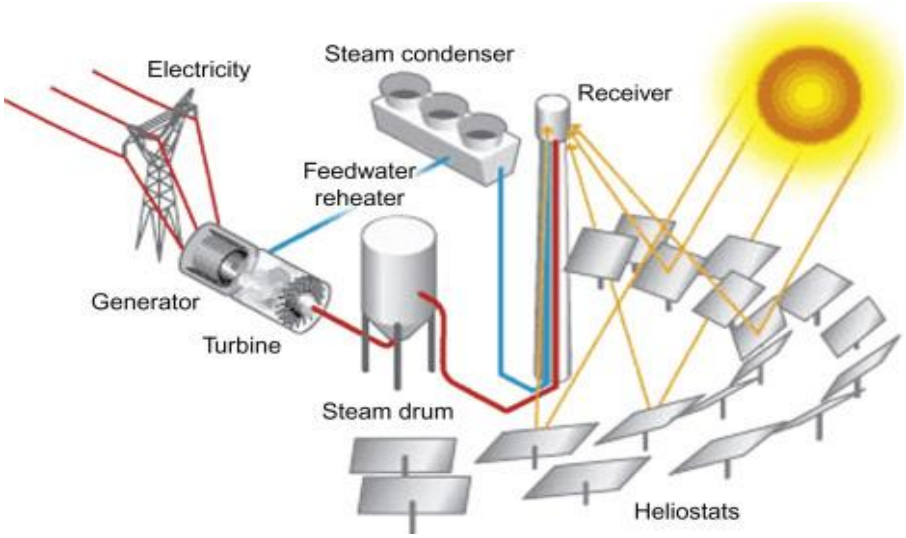

Figure I.11. *Heliostat field collector.*

I.6.3.c Parabolic Dish Reflector (PDR) :

It is a point-focus collector that tracks the sun in two axes, concentrating solar energy onto a receiver located at the focal point of the dish. The dish structure must track fully the sun to reflect the beam into the thermal receiver.

The receiver absorbs the radiant solar energy, converting it into thermal energy in a circulating fluid. The thermal energy can then either be converted into electricity using an engine-generator coupled directly to the receiver, or it can be transported through pipes to a central power conversion system. Parabolic dish systems can achieve temperatures in excess of 1500 °C.

Parabolic dishes have several important advantages:

- ✓ Because they are always pointing at the sun, they are the most efficient collector systems.
- ✓ Typically, they have a concentration ratio in the range of 600–2000 and are highly efficient at thermal-energy absorption and power conversion systems.
- ✓ They have modular collector and receiver units that can either function independently or as part of a larger system of dishes.

Parabolic-dish systems that generate electricity from a central power converter collect the absorbed sunlight from individual receivers and deliver it via a heat-transfer fluid to the power-conversion systems. The need to circulate heat transfer fluid throughout the collector field raises design issues, such as piping layout, pumping requirements, and thermal losses. The Stirling engine is the most common type of heat engine used in dish-engine systems. For this system, certain level of reliability and mass production still need to be achieved.

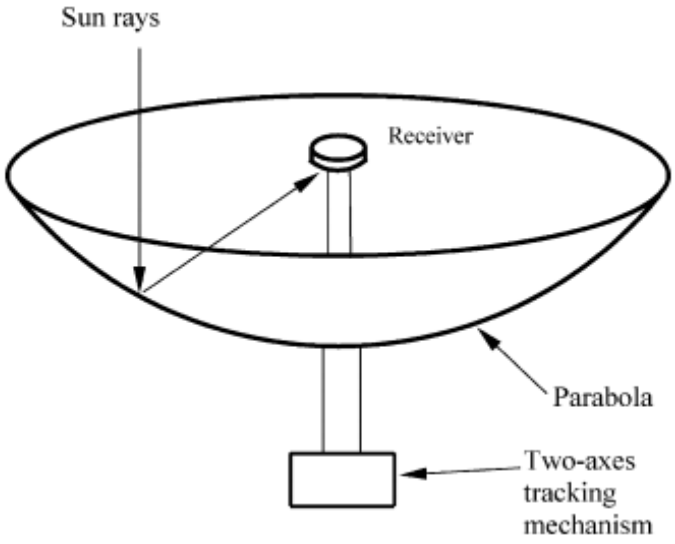

Figure I.12: *Parabolic concentrator.*

I.6.4 Application of solar concentrator:

I.6.4.a Electric generator (Solar parabolic dish Stirling engine system):

The main use of this type of concentrator is for parabolic dish engines. A parabolic dish-engine system is an electric generator that uses sunlight instead of crude oil or coal to produce electricity. The major parts of a system are the solar dish concentrator and the power conversion unit.

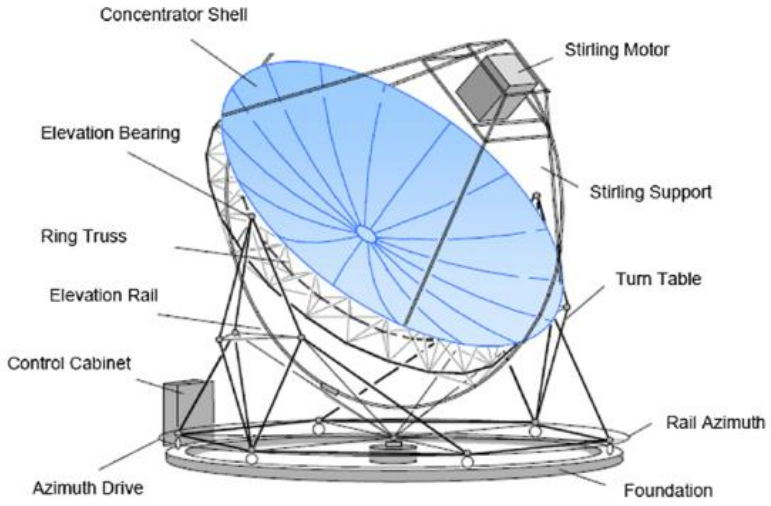

Figure I.13: *Design view of parabolic dish ‘‘EURODISH” TM”*[9]

The parabolic dish systems consists of a parabolic reflector in the form of a dish with a supporting structure, Stirling engine mounted in the focus of the parabolic dish to receive solar 62 A.Z. Hafez et al. / Energy Conversion and Management 126 (2016) 60 – 75 radiation, and a generator to generate electrical energy. Throughout the day, solar parabolic dishes is directed toward the sun automatically using tracking control system. In this section, the system design is presented. Two types for solar parabolic dish systems and components [10]are shown in **(Figures**. **13** and **14**) The parabolic dish ‘‘EURODISH” TM” is a 10-kilowatt-electrical (kWe) solar dish Stirling (DS) system, shown in (**Figure I.13)**. The parabolic dish ‘‘The SunCatcherTM” is a 25-kilowatt-electrical (kWe) solar dish Stirling (DS) system, shown in (**Figure I.14):**[11]

The system description can be divide it to three main parts:

1. Solar dish concentrator and structure.
2. Stirling engine and receiver.
3. Solar tracking system.

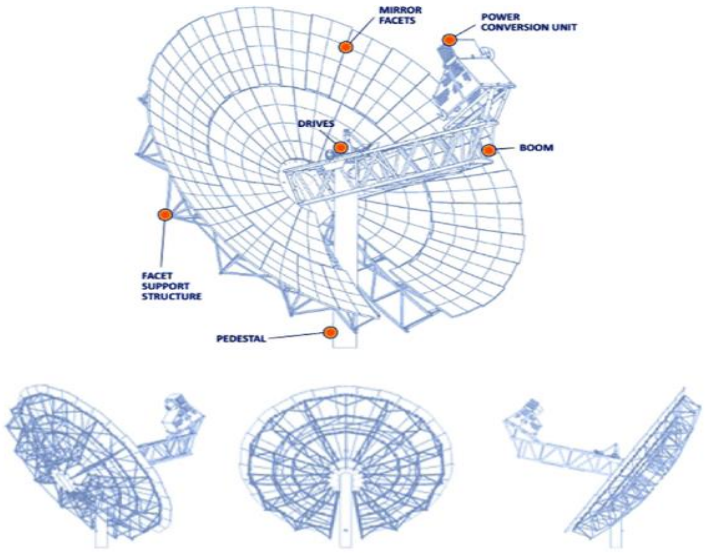

Figure I.14:*Design view of parabolic dish "The SunCatcher TM* "[12].

I.6.4.b Solar water heater*:*

The solar water heating system consists of a parabolic dish concentrator, conical heat absorber, water heater and water as a working fluid. A schematic of solar water heater with parabolic dish and conical heat absorber is shown in **(Figure I.15).** The experimental model is suitable for open ground to have a better view of the sun‘s radiation. The parabolic dish collector was constructed with aluminum sheet because of low weight, ease of fabrication and energy

efficiency. To reduce the weight of the dish, a light glass mirror of 2 mm thickness, of high surface quality and good specular reflectance was used[13].

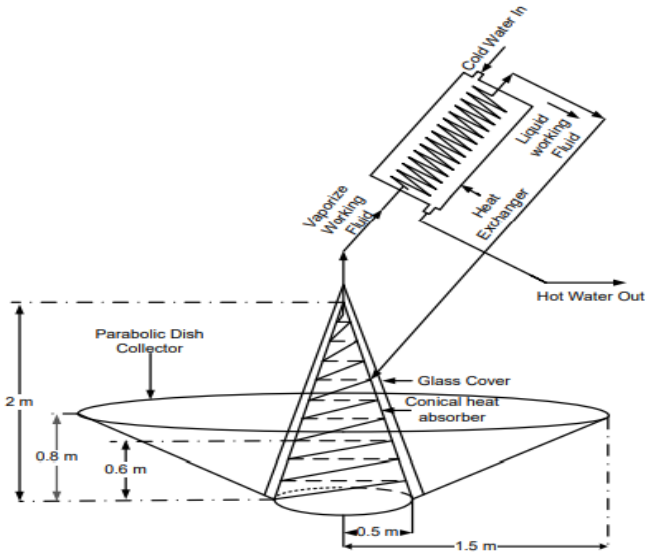

Figure I.15:*Schematic of solar water heater system*[14].

I.6.4.c Realization of a CVD Spray frame assisted by solar concentrator:

In this our work we used the solar concentrator **(Figure I.16)** to help us for the manufacture of thin films using pyrolysis spray technology and solar heating mode to replace the expensive electric method.

This deposition method uses solar radiation as a heat source.

The objectif of using the solar concentrator in the manufacture of thin films are:

- ✓ Realization of a CVD Spray frame assisted by solar heating (oven).
- ✓ Optimization of deposition parameters (solution concentration).

Figure I.16: *General view of the solar concentrator used (laboratory22, Echahid Hamma Lakhdar University, El Oued).*

I.7 Conclusion:

In this chapter, we learned about the structure and characteristics of the sun, energy and radiation at ground level. Some of the astronomical data needed for this study were identified and we provided. Some data on the solar field in Algeria, and again a description of a solar collector plane of air; also we talked about our concentrator experimental used.

II *Chapter* II

Thin films

NiO-Co and deposition techniques

II.1 Introduction:

At the beginning of this chapter, we will present generalities on thin layers then we will cite some methods of their physical and chemical deposits as well as the properties of the chosen chemicals, we will finally expose the spray pyrolysis process.

II.2 Definition of the thin film:

A thin film is a layer of material ranging from fractions of a nanometer (monolayer) to several micrometers in thickness". Many of the electronic semiconductor devices are the main applications benefiting from thin film construction. The semiconducting material, in thin film form are of particular interest because it has a various number of applications viz.

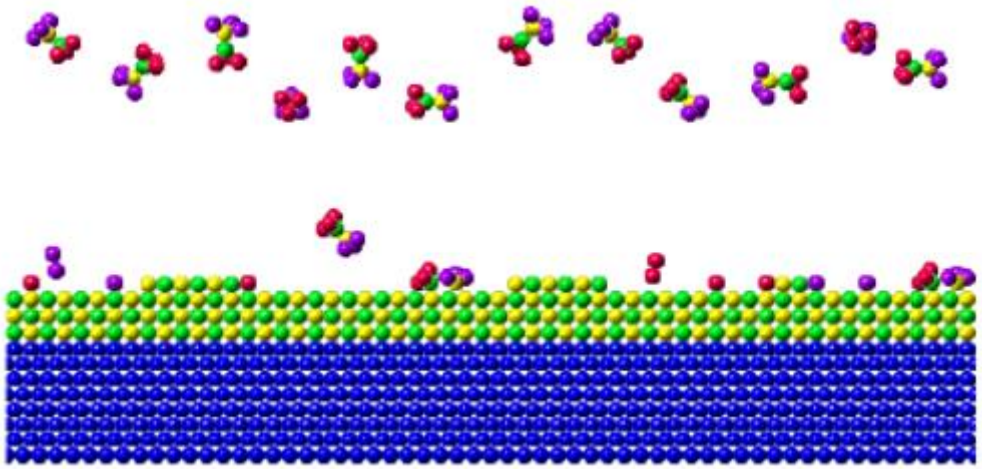

Figure II.1: *Thin layer deposition on the* substrate.

Thin film plays an important role in the nanotechnology and nanoscience development. Solar cell is an important application of thin film technology from the point in view of global energy crunch, which converts the energy of the solar radiation into useful and constructive electrical energy.

II.3 Thin-Film Applications:

In considering the different applications of deposited thin films, the following generic categories can be identified.[15]

Electronic Components*:* The fabrication of electronic components ,especially solid-state devices and microelectronic integrated circuits, have undoubtedly found the widest and most

demanding applications for thin film depositions. These films typically consist of semiconductor materials, dielectric and insulating materials, and metal or refractory metal silicide conductors.

Electronic Displays: Electronic displays are used for interfacing electronic equipment with human operators. Different components and device structures are required, such as:

- Liquid-crystal displays.
- Light-emitting diodes (LEDs).
- Electroluminescent displays.
- Plasma and fluorescent displays.
- Electrochromic displays.

The fabrication of these displays requires conductive films, transparent and conductive films, luminescent or fluorescent films as well as dielectric and insulating layers.

Optical Coatings: Optical coatings are applied for antireflection purposes, as interference filters on solar panels, as plate glass infrared solar reflectors, and for laser optics. In the fabrication of filter optics, thin films with refractive index gradients are deposited on preforms from which the optical fibers are drawn. These coatings require dielectric materials with precisely defined indices of refraction and absorption coefficients. Laser optics require metal reflective coatings which can withstand high radiation intensities without degradation. Infrared reflecting coatings are applied to filament lamps to increase the luminous flux intensity.

Magnetic Films for Data Storage: Thin films of magnetic materials have found wide commercial applications for data storage in computers and control systems. The substrates can be metal, glass or plastic polymeric materials. Thin film deposition processes for magnetic materials and for materials with a high degree of hardness are required.

Optical Data Storage Devices: Thin films are finding increasing commercial use for optical data storage devices in compact disks and computer memory applications. Processes for the deposition of organic polymer materials as storage media and as protective overcoats are required for this technology.

Antistatic Coatings: Thin films of conductive or semi-conductive materials are deposited to provide protection from electrostatic discharges.

Hard Surface Coatings: Thin film coatings of carbides, silicides, nitrides, and borides are finding increased uses to improve the wear characteristics of metal surfaces for tools, bearings, and machine parts. Of particularly great current interest are films of diamond-like carbon because of this material's heat dissipation properties, electrical insulation, hardness, and resistance to high-temperature and high-energy radiation.

II.4 Definition of Nickel oxide (NiO):

Nickel (II) oxide is the chemical compound with the formula$\boldsymbol{NiO}$. It is the principal oxide of nickel.[16] It is classified as a basic metal oxide. Several million kilograms are produced annually of varying quality, mainly as an intermediate in the production of nickel alloys.[17] The mineralogical form of NiO, bunsenite, is very rare. Other nickel (III) oxides have been claimed, for example: Ni_2O_3andNiO_2.

$\boldsymbol{NiO}$ Can be prepared by multiple methods. Upon heating above 400 °C, nickel powder reacts with oxygen to give$\boldsymbol{NiO}$. In some commercial processes, green nickel oxide is made by heating a mixture of nickel powder and water at 1000 °C, the rate for this reaction can be increased by the addition of $\boldsymbol{NiO}$.[18]

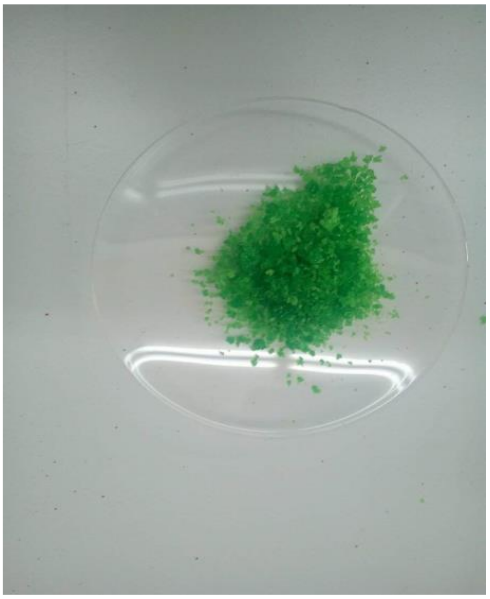

Figure. II.2: *Hydrated nickel chloride.*

$\boldsymbol{NiO}$ Adopts the $\boldsymbol{NaCl}$ structure, with octahedralNi^{2+} and O^{2-} sites. The conceptually simple structure is commonly known as the rock salt structure. Like many other binary metal oxides, NiO is often non-stoichiometric, meaning that the $Ni{:}O$ ratio deviates from1:1. In

nickel oxide, this non-stoichiometry is accompanied by a color change, with the stoichiometrically correct NiO being green and the non-stoichiometric $\boldsymbol{NiO}$ being black.

II.4.1 Properties of hydrated nickel chloride:

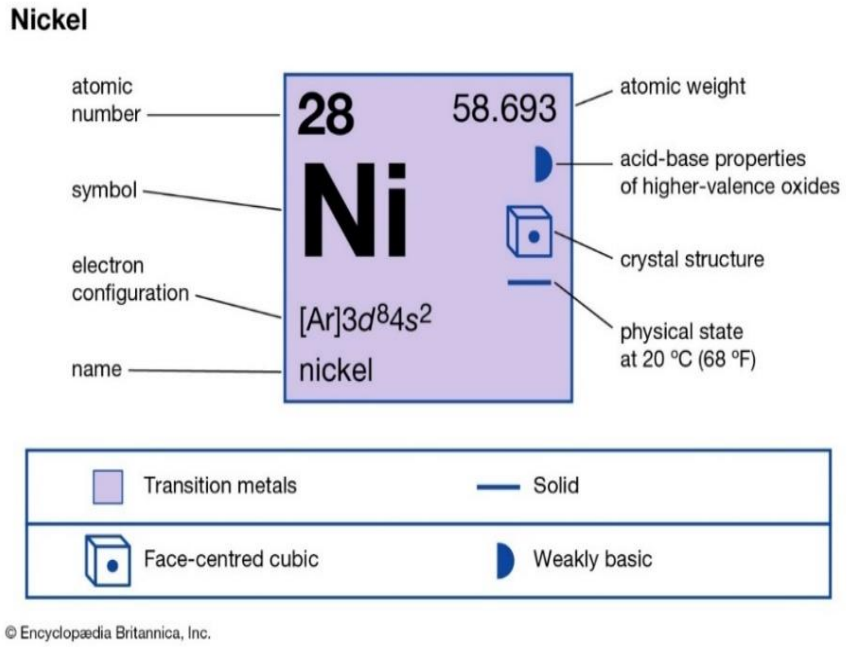

Figure II.3: *Properties of **Nickel (Ni)** element[19]*

.

Table II.1: *The table shows element percentages for NiO (nickel oxide).[20]*

Element	%
Ni	78,58
O	21,42

NiO is an attractive p-type transparent semiconductor that is being explored for a variety of applications. We report a systematic study of the electronic properties, relevant to hole-transporting materials in solar energy conversion applications, of NiO synthesized by atomic layer deposition (ALD).[21]

Table II.2*: Some general properties of NiO.*

Average atomic number	18
Average atomic mass **(g)**	27.35
Molar mass **(g / mol)**	74.69
Boiling point **(° C)**	>2000
Solubility in water **(mg / L)**	1.1 at 20 ° C. insoluble
Melting point **(° C)**	1990 - 1960
Enthalpy of formation at 298k	-240 KJ / mole of atoms
Entropy S_0 **(JK-1.mol-1)**	38.00

II.4.1.a *Crystallographic properties:*

Nickel oxide (NiO) crystallizes in a cubic structure of the $NaCl$ type (rocksalt) shown in the figure. It has an elementary mesh with parameters a = 4.117 Å, separated by an angle of 90°. It belongs to the space group$Fm3m$, in which the nickel atoms are in an octahedral coordination with six oxygen atoms, with a density of 6.67g / cm^3.[3]

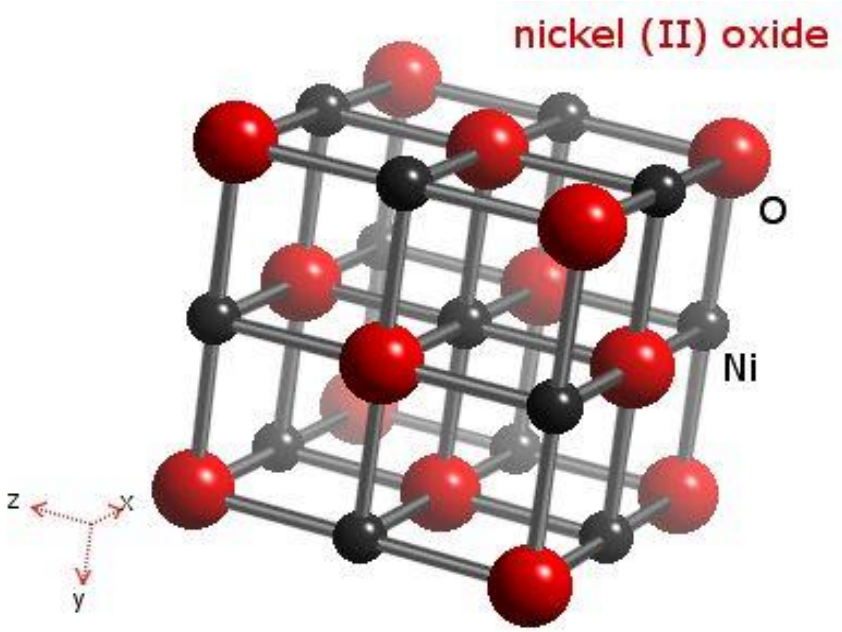

Figure II.4:*Crystallographic structure of nickel oxide*.[22]

II.4.1.b Electronic properties:

The electronic properties of NiO (1 1 0)/MAPbI3 (1 0 0) interface are investigated by the first-principles calculations. The NiO (1 1 0)/MAPbI3 (1 0 0) interfacial lattice mismatch is 7.3%. The binding energy of the NiO (1 1 0)/MAPbI3 (1 0 0) interface is -0.059 J/m^2, and the atoms bonding is irregular at the interface. There are some interface states nearby the NiO (1 1 0)/MAPbI3 (1 0 0) interface. Interface states of the NiO (1 1 0)/MAPbI3 (1 0 0) interface mainly are attributed to I-5p, O-2p and Ni-3d orbitals on the MAPbI3 (1 0 0) layer1 and NiO (1 1 0) layer1.[23]

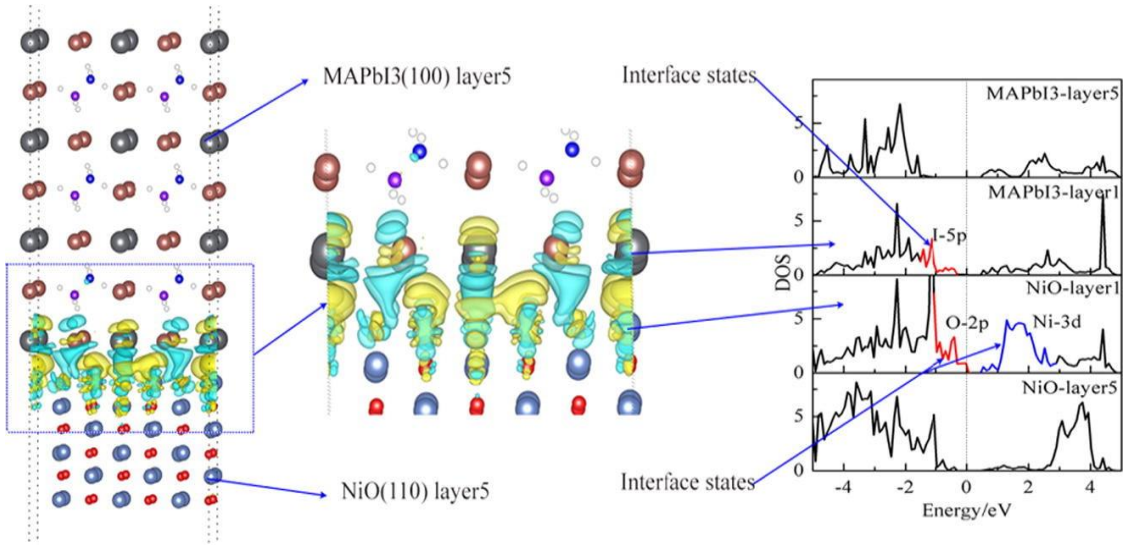

Figure II.5: *The charge density difference (a) and partial enlarged view (b) of the NiO (1 1 0)/MAPbI3 (1 0 0) interface.*

II.4.1.c Electrical Properties of Nickel Oxide:

The electrical properties of nickel oxide have been studied extensively by many investigators. Morin[24] and van Houten[25] have discussed the electronic structure of this oxide and have shown that NiO has no 3d band but full, localized $3d^8$ levels (Ni^+ levels) and empty $3d^9$ levels (Ni^+levels).

According to van Houten the $3d^9$ levels are situated 5.4 eV above the $3d^8$levels which lie about 5.3 eV above the filled O^{2-} band.

The energy difference between the Ni^{2+} and Ni^+ levels is too large for pure stoichiornetricNi0 to behave like an intrinsic semiconductor at ordinary temperatures, and as electron transfer

between the full localized $3d^8$ levelsis not possible, pure NiO is an insulator at room temperature with a conductivity of $\sigma<10^{-13}\Omega^{-1}.cm^{-1}$.[26]

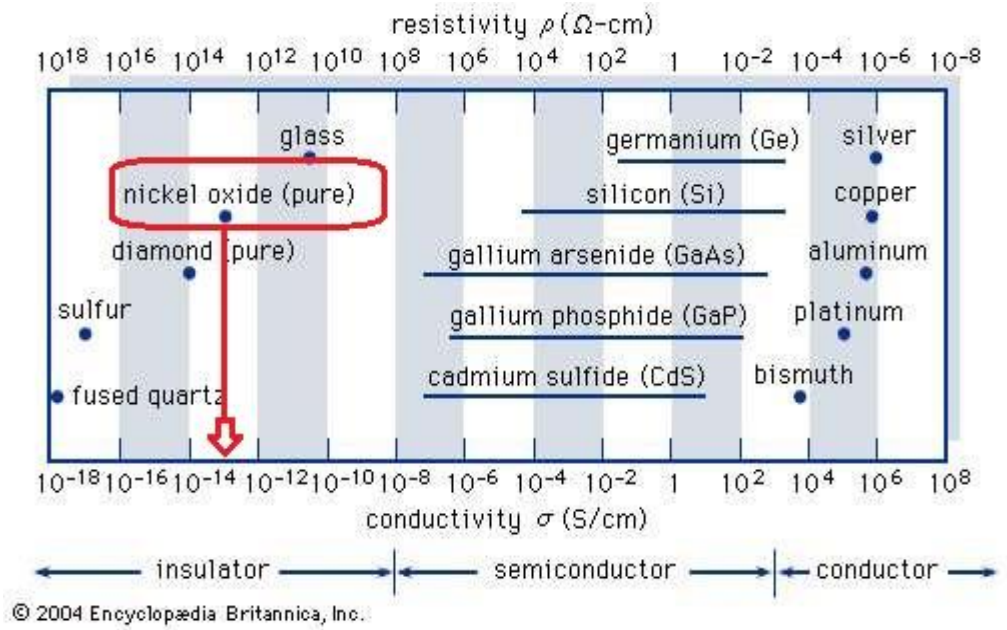

Figure II.6:*Typical range of conductivities for insulators, semiconductors, and conductors*.[27]

Table II.3: *Some electrical properties of NiO.*

Conductivity $\boldsymbol{\sigma}$ $(\boldsymbol{\Omega}.\mathbf{Cm})^{-1}$	≤ 0.1
Mobility $\boldsymbol{\mu}$ $(\boldsymbol{cm^2/V.S})$	0.1^{-1}
Electronic densities $\boldsymbol{N}$ $(\boldsymbol{cm^3})$	$10^{18} - 10^{19}$
Prohibited band energy $\boldsymbol{Eg}$ $(\boldsymbol{eV})$	$3.5ev - 4ev$
Dielectric constant	11.9

II.4.1.d Optical properties of Nickel Oxide:

The optical reflectance spectra of the transition-metal oxides NiO and CoO have been measured over the energy range from 1 to 26 eV. The optical constants have been derived by means of a Kramers-Kr5nig analysis of their reflectance spectra. Structure in reflectance is found at 4. 0, 4. 8, 5.9, 7. 2, 8. 25, 12.8, 13.6, and 17.8 eV in NiO, and at 5.5, 7. 5, 12.6, and 17.5 eV in CoO. The positions of high-energy structure in their absorption coefficients is consistent with maxima

in their respective optical densities of states determined from photoemission data. Two alternative interpretations are given for the structure in NiO between 4.0 and 9.0 eV. One interpretation involves oxygen p and nickel d states in localized excitations, and the other

Involves the nickel d states and the "4s"band. Distinction between models on the basis of presently available photoconductivity data is found to be questionable.[28]

II.4.2 Properties of Cobalt:

Cobalt is a well-known hard magnetic material and its compounds are widely used for variety of applications in computer, electronic, and medical industries [29] It is one of the most interesting magnetic materials due to its large magnetocrystalline anisotropy that lies along the c-axis. Various parameters including shape, size, and texture strongly influence magnetic properties of cobalt nanowires. Theseparameterscanbecontrolledduring fabrication process[30] .

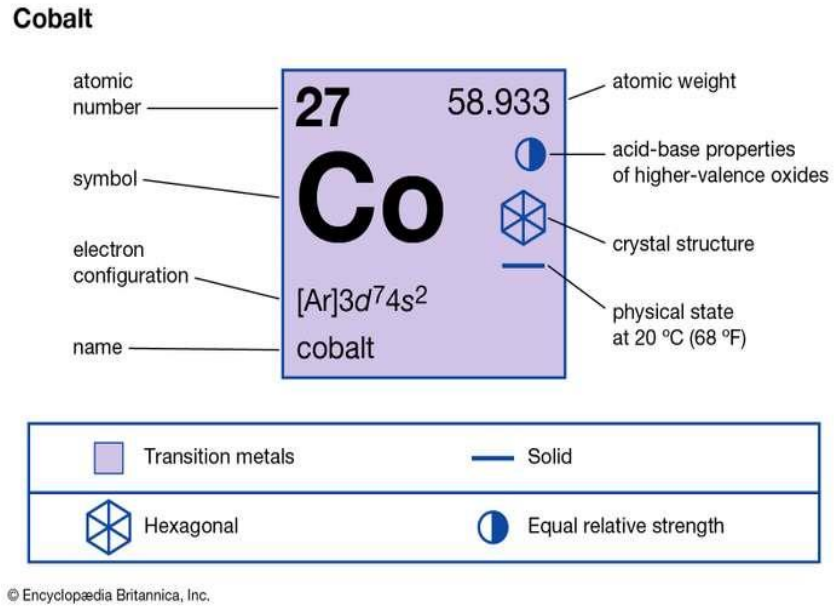

Figure II.7:*Properties of* ***Cobalt (Co)***[19]

Table II.4*: Properties of Cobalt (Co).*

electron configuration	**[Ar]3$d^7$4s^2**
atomic number	**27**
atomic weight	**58.9332**
melting point	**1,495 °C (2,723 °F)**
boiling point	**2,870 °C (5,198 °F)**
density	**8.9 g**/cm^3 **at 20 °C (68 °F)**
oxidation states	**+2, +3**

II.4.2.a Crystallographic properties of Cobalt :

- Geometry of cobalt: 6 coordinate: octahedral
- Prototypical structure: NaCl (rock salt)

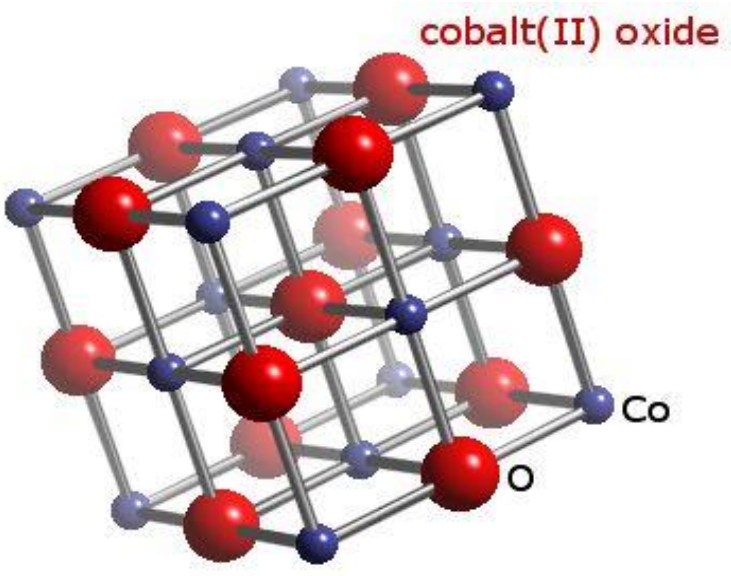

Figure II.8: *Crystallographic structure of Cobalt*[31]

Table II.5: *The table shows element percentages for* $CoCl_2.6H_2O$ *(hexaaquocobalt dichloride)[32]*

elements	symbol	Atomic Mass	*Of Atoms	Mass percent
Chlorine	Cl	35.453	2	29.801%
Cobalt	Co	58.933200	1	24.769%
Hydrogen	H	1.00794	12	5.084%
Oxygen	O	15.9994	6	40.346%

II.4.3 Role of dopants in metal oxides

Doping is the process of adding some foreign substance into the semiconductor. These added foreign substances are known as dopants. Dopants may be cationic (addition of cation to metal oxide) such as Co, Cr, Fe, Ni etc., or anionic (addition of anion to metal oxide) such as C, N, S etc. (Ali et al., 2012). Usually doping is done in metal oxides to create tail states in the

Vicinity of the valence band, which leads to decrease in effective band gap. Actually, doping of metal oxides like TiO2, ZnO with metal and/or transition metals increases the surface defects, which ultimately increases the surface area. These surface defects and increased surface area play an important role in the catalytic activities of metal oxides (Ullah and Dutta, 2008). Doping of metal oxide semiconductors causes the following key changes in the band gap electronic structures as summarized by Serpone, 2006.

- Increased localize dopant levels near the conduction and valence bands
- Band gap shrinkage due to broadening of the valence band
- Localized dopant levels and electronic transitions to the conduction band
- Electronic transitions from localized levels near the valence band to their corresponding excited states

Thus, dopants play a key role to achieve technologically important desired properties in the semiconductors[33].

Figure II.9: *Doping metal oxides (cobalt-nickel).*

II.5 Deposition technique :

The wide classification of thin film deposition techniques is showed in **(Figure II.10)**[34].

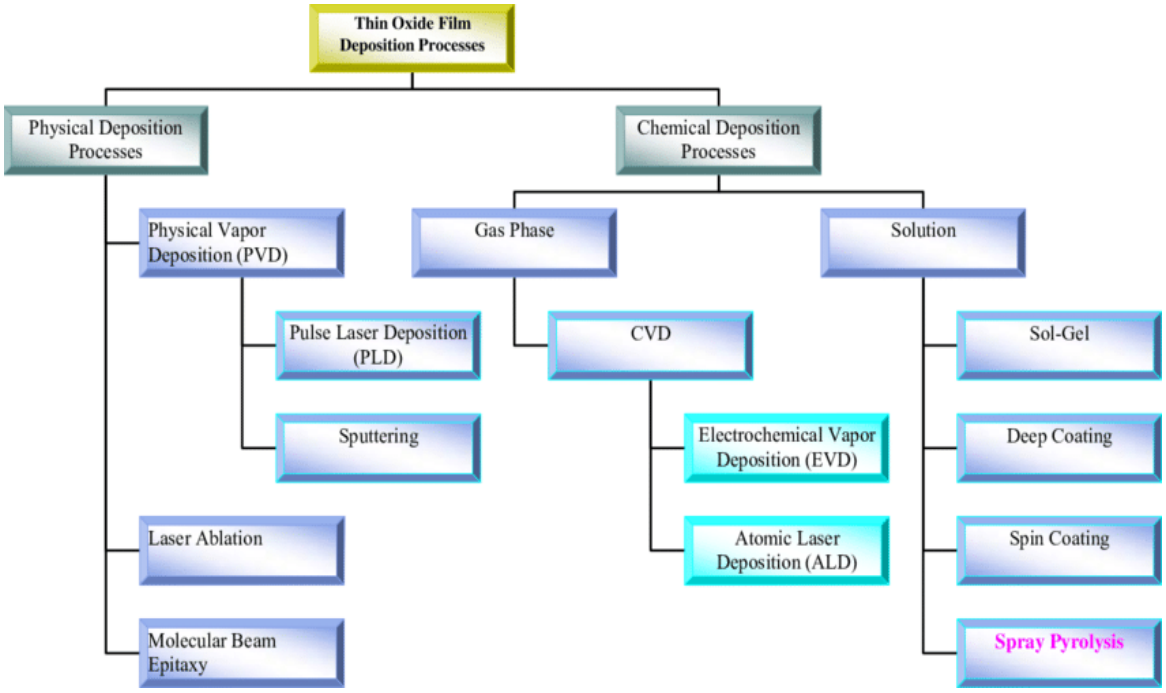

Figure II.10: *Schematic diagram of thin film deposition*[35].

II.5.1 Physical vapor deposition (PVD) :

Physical vapor deposition (PVD) processes (**Figure II.11)** are deposition processes in which atoms or molecules of a material are vaporized from a solid or liquid source, transported in the form of a vapor through a vacuum or low-pressure gaseous environment, and condense on a substrate. PVD processes can be used to deposit films of elemental, alloy, and compound materials as well as some polymeric materials.

PVD processes can be categorized as follows:

Vacuum evaporation--material from a thermal vaporization source reaches the substrate without collision with gas molecules in the space between the source and substrate. Sputter deposition--sburce of vaporized material is a surface (target) being subjected to physical sputtering. As far as film properties are concerned sputter deposition should be further subdivided into high- and low-pressure sputter deposition. Arc" vapor deposition--uses a high current, low-voltage electric arc in a low-pressure gas to erode the solid cathodic electrode by a moving arc or to melt and evaporate the anodic electrode.

Ion plating--utilizes concurrent or periodic bombardment of the depositing film by atomic-sized energetic particles to modify and control the composition and properties of the depositing film. Ion plating can use vacuum evaporation sputtering or arc vaporization as the source of the depositing material. Ion beam assisted deposition (IBAD) uses a high-energy ion beam to bombard the depositing film with inert or reactive ions to modify the film properties and, in the case of a reactive ion, to enhance chemical reactions. (**Figure II.11)** summarizes the various PVD processes.

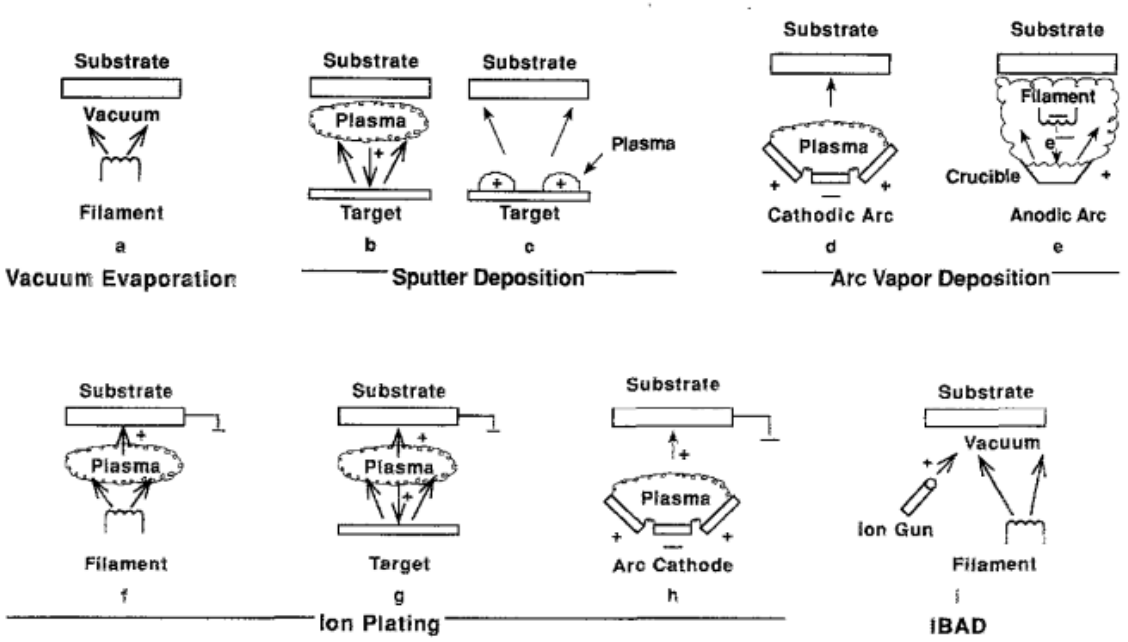

Figure II.11 : *Schematic views PVD processing technique[36].*

II.5.2 Chemical Vapor Deposition (CVD) :

II.5.2.a Introduction to Chemical Vapour Deposition :

Being an effective way of constructing a wide range of components and products with potentially different material composition, chemical vapour deposition (CVD) has been developed since its inception as a novel manufacturing process in several industrial sectors. Notably, these include the semiconductor industry, ceramic industry and so forth. A trend of expanding its applications from initial mass semiconductor and microelectronics production to a wider range of applications has gained momentum in recent years as a result of intensive research and development work being undertaken by academic researchers and industrial end-users.[37]

II.5.2.b Definition of CVD *:*

Chemical vapor deposition may be defined as the deposition of a solid on a heated surface from a chemical reaction in the vapor phase. It belongs to the class of vapor-transfer processes which is atomistic in nature that is the deposition species are atoms or molecules or a combination of these. Besides CVD, they include various physical-vapor deposition processes (PVD) such as evaporation, sputtering, molecular beam epitaxy, and ion plating[38] Chemical Vapor Deposition (CVD) has developed into one of the fundamental technologies of the

semiconductor industry. The key to understanding the CVD process is the Boundary Layer Theory (BLT), which explains how the CVD reaction takes place. With a broad understanding of BLT, the process engineer can make intelligent adjustments to a complex process. An understanding of BLT becomes essential for the semiconductor engineer as he looks into new CVD techniques in epitaxial, mid-temperature, low temperature, and plasma-enhanced deposition.[39]

Chemical vapor deposition (CVD), with its many variations, is an important thin-film deposition technique. In conventional CVD, the constituents of the film to be deposited are introduced into a reaction chamber as a vapor or gas. In many cases, the precursors are liquids or solids and must be heated at low pressure to contribute enough vapor to produce reasonably rapid deposition rates. In some cases, certain precursors are unstable and decompose under these conditions. Many such CVD precursors are expensive. The deposition of multielement coatings usually requires a complex system to handle the various elemental precursors.[40]

(Figure II.12 a): gives a typical example of a CVD system, where reactant gases, normally called precursor gases of CH_3SiCl_3 andH_2 , are delivered into a reaction chamber at a suitably determined temperature. As they pass through the reactor these gases come into contact with a heated substrate; they then react and form a solid SiC layer deposited onto the surface of a substrate. Usually, an inert gas, such as Ar, is used as a diluent gas. The depositing temperature and pressure are the critical parameters in this process. After the reactions, the exhaust gases containing HCl species are trapped by NaOH and then condensed by liquid N2 trap before being released into the atmosphere.

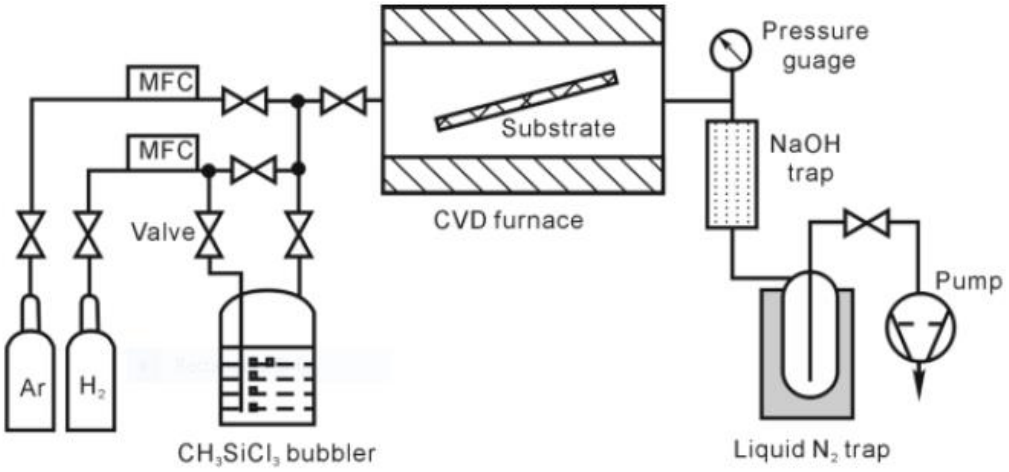

Figure II.12 a: *Schematics of a CVD process: arrangement of a CVD system*

CVD is therefore a generic name for a group of processes that involve forming a thin layer via chemical reaction and depositing a solid material layer onto substrates.

Figure II.12b: shows a model consisting of the sequential physical and chemical steps that occur during a CVD process, developed by Spear in 1982 [41]. They are summarized as follows:

1. Mass transport of reactant gaseous species to vicinity of substrate;
2. Diffusion of reactant species through the boundary layer to the substrate surface or homogeneous chemical reactions to form intermediates;
3. Adsorption of reactant species or intermediates on substrate surface;
4. Surface migration, heterogeneous reaction, inclusion of coating atoms into the growing surface, and formation of by-product species;
5. Desorption of by-product species on the surface reaction;
6. Diffusion of by-product species to the bulk gas;
7. Transport of by-product gaseous species away from substrate (exhaust).

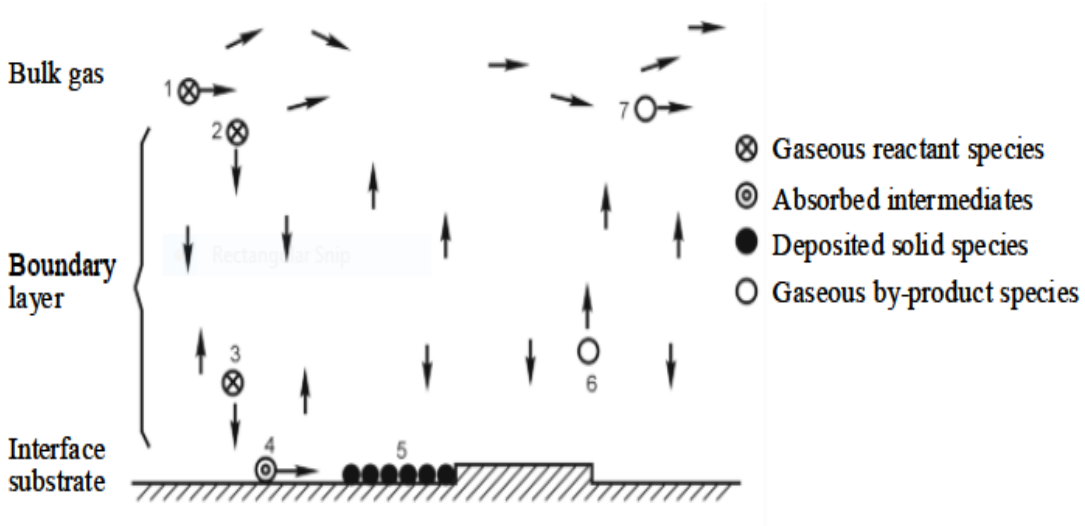

Figure II.12b: *Schematics of a CVD process: a CVD model.*

II.6 Spray pyrolysis:

Spray pyrolysis is a processing technique being considered in research to prepare thin and thick films, ceramic coatings, and powders. Unlike many other film deposition techniques, spray pyrolysis represents a very simple and relatively cost-effective processing method (especially

with regard to equipment costs). It offers an extremely easy technique for preparing films of any composition. Spray pyrolysis does not require high-quality substrates or chemicals. The method has been employed for the deposition of dense films, porous films, and for powder production. Even multilayered films can be easily prepared using this versatile technique. Spray pyrolysis has been used for several decades in the glass industry and in solar cell production.

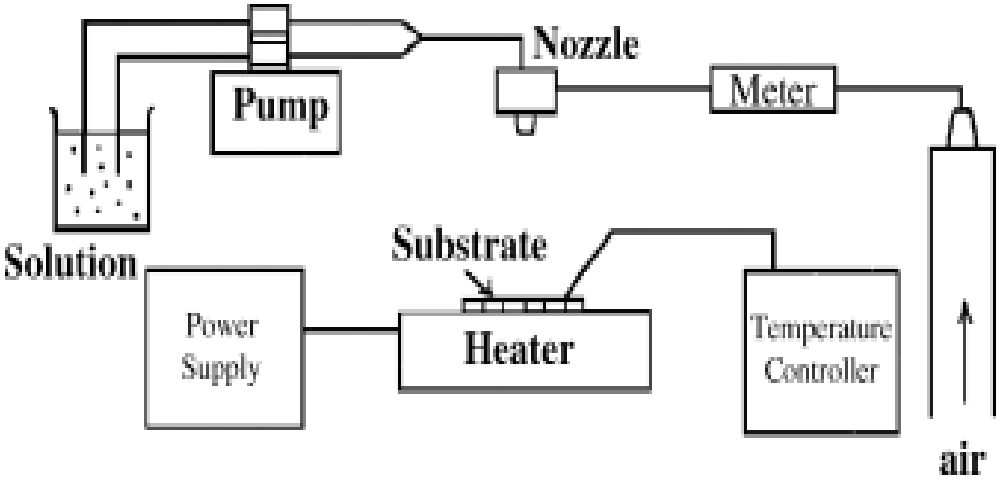

Figure II.13. *Schematic diagram of the spraying system*.[42]

Typical spray pyrolysis equipment consists of an atomizer, precursor solution, substrate heater, and temperature controller. The following atomizers are usually used in spray pyrolysis technique: air blast (the liquid is exposed to a stream of air), ultrasonic (ultrasonic frequencies produce the short wavelengths necessary for fine atomization) and electrostatic (the liquid is exposed to a high electric field).[43]

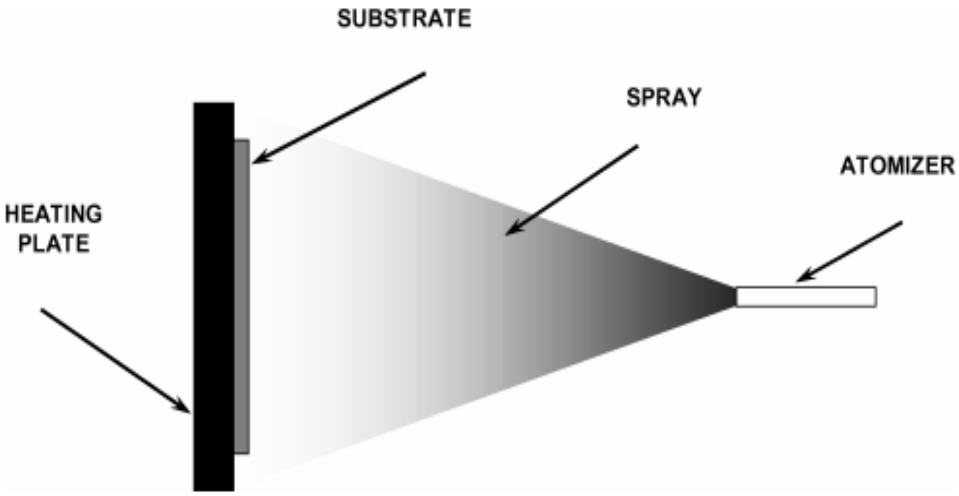

Figure II.14. *Schematic diagram of spray pyrolysis equipment.*

II.7 Conclusion :

In this chapter, we presented the different structural, electronic, optical and electrical properties of the thin layers of NiO and Co. In the second part of this chapter, we learned the techniques of PVD and CVD, the dopant process, and finally we talked about the principle of spray pyrolysis deposition.

III Chapter III:

Techniques for Elaboration and characterizing thin films

III.1 Introduction:

In this chapter, first we have deposited thin layers in our laboratory by the spray pyrolysis method on glass substrates. And gives us a definition and the mechanism of formation of this thin layer. Also some thin film characterization methods like (x-ray diffraction, UV-Visible spectroscopy and electrical characterization).

III.2 Elaboration of thin films of Co doped NiO:

III.2.1 General principle of the spray process:

A solution of different reactive compounds is vaporized, using an atomizer, on a heated substrate. The temperature of the substrate allows the activation of the chemical reaction between the compounds[44]The experiment can be performed in air[45]The choice of this technique was motivated in view of many advantages[46]:

- A wide choice of precursors is possible, the compound must be soluble in a solvent, so the solution can be atomized.
- Possibility of depositing a wide choice of materials.
- Simple method of supplying the precursor by means of a spray.
- High growth speed because the mass transport of the precursor can be very high.
- Reaction environment simply controllable, under neutral gas or under air at atmospheric pressure.
- Ease of making reactors of this type.

III.2.2 Experimental setup used:

It is a frame produced in the laboratory 22 of Mechanical engineering of the University of El Oued and made from simple elements to which we have made modifications so as to produce films of Nickel-Cobalt with new way.

The solar concentrator is composed of the following elements:

1. Reflector
2. Receiver
3. Support
4. The tracking system

5. The multimeter.
6. Compressor
7. Atomizer

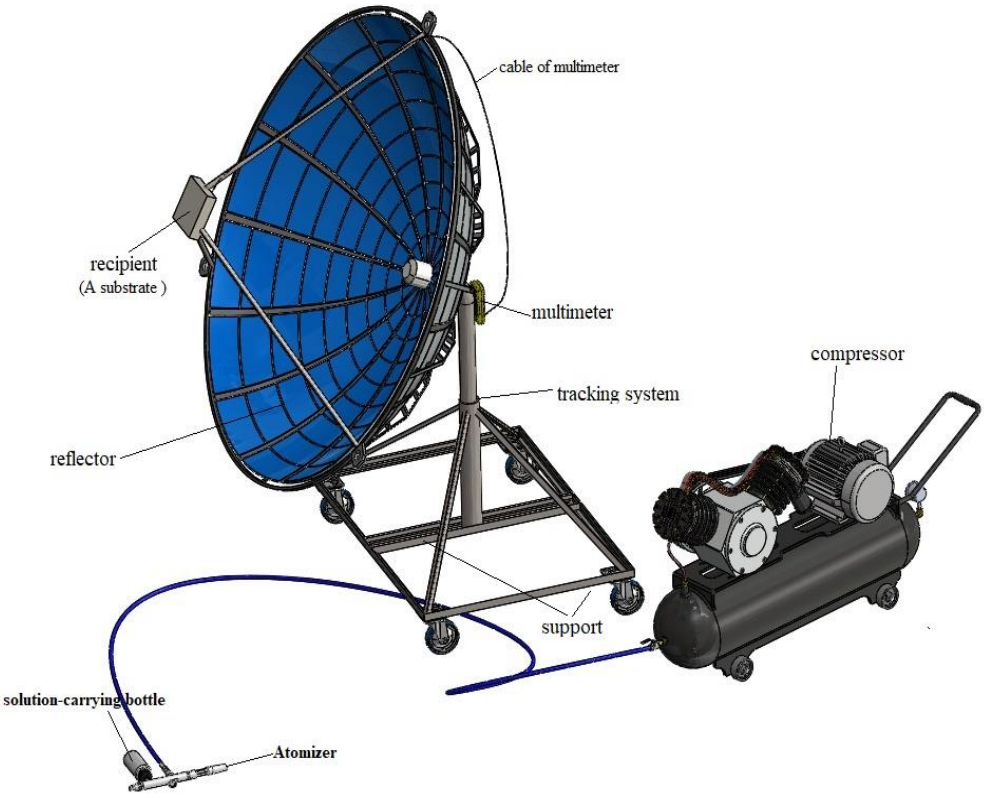

Figure III.1: *Complete assembly of the solar oven used.(Designed by Solidworks)*

III.2.2.a Description of the elements of the device:

- **A reflector:** It is a parabola of satellite receiver covered by a hundred small surfaces of mirrors which cover the interior surface of the reflector. Mirrors should have their bright side facing the sun (figure).

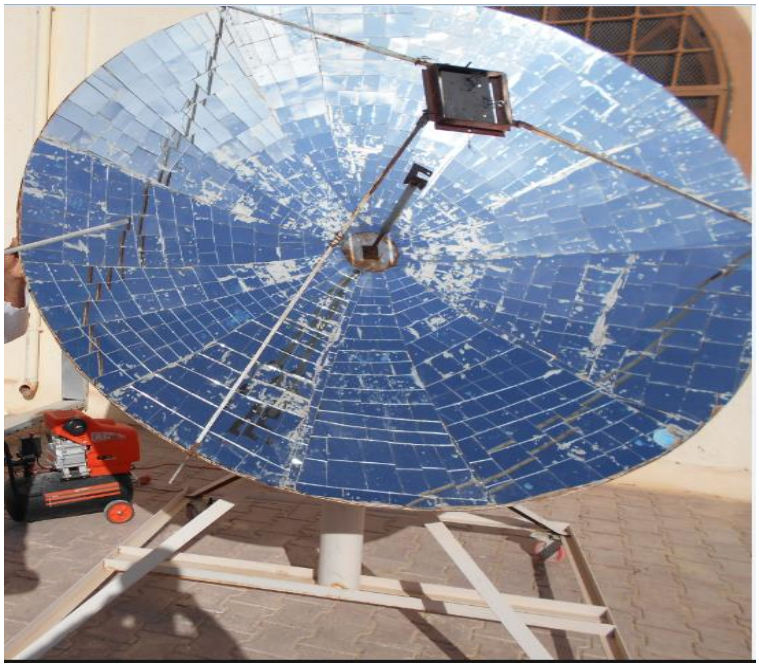

Figure III.2 : *satellite receiver dish.*

- **A substrate holder:** this is a 15 cm long tray (**Figure III.3)** , heated by solar energy, the temperature of which can be regulated using a temperature controller which is connected to a multimeter of the type (VCA61A - LCD).

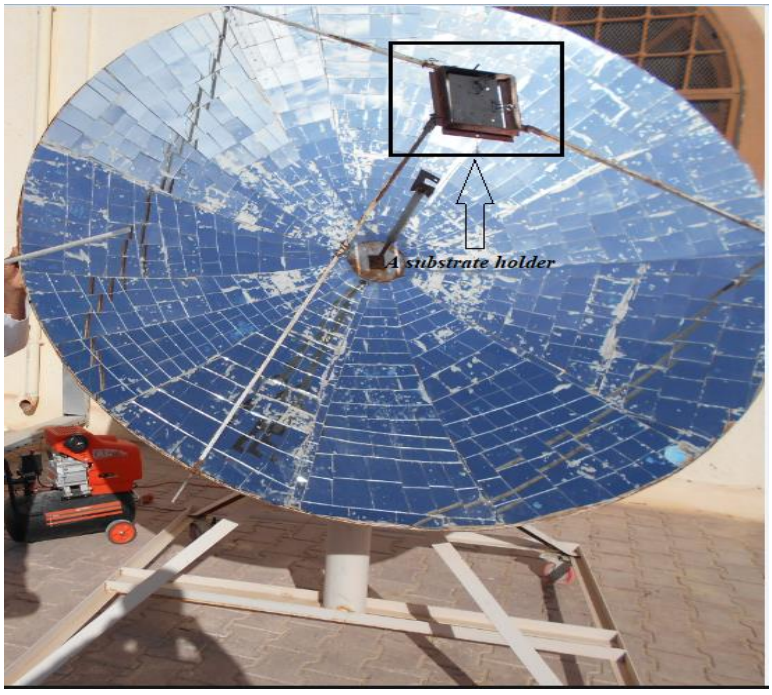

Figure III.3: *a substrate holder.*

This temperature can be set at room temperature and increases up to ≈1000°C (**Figure III.4**).

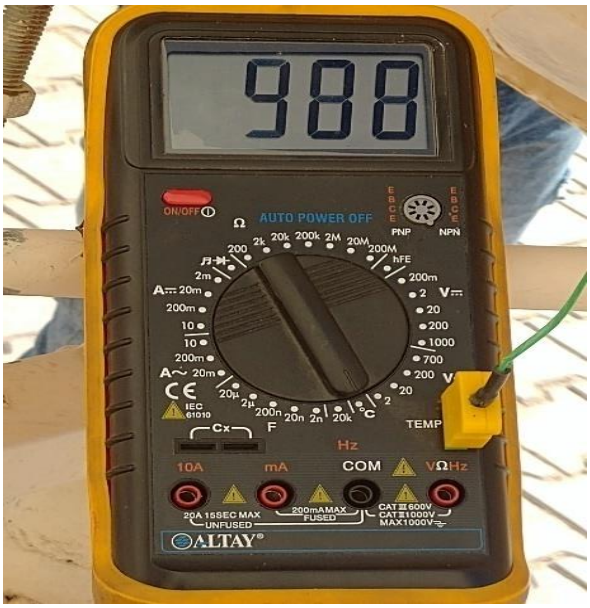

Figure III.4: *temperature and increases up*.

- **A solution-carrying bottle:** feeds by gravity a low-flow atomizer (**Figure III.5)**.
- **Atomizer:** It is an element which transforms the solution into droplets. It is placed on a height-adjustable support to control the distance between the substrates (**Figure III.5)**.

Figure III.5: *the atomizer with the solution-carrying bottle.*

III.2.3 The solutions used:

Doping means the introduction of impurities into a semiconductor crystal to the defined modification of conductivity.

The dopant is integrated into the lattice structure of the semiconductor crystal, the number of outer electrons define the type of doping. Elements with 3 valence electrons are used for p-type doping, 5-valued elements for n-doping.

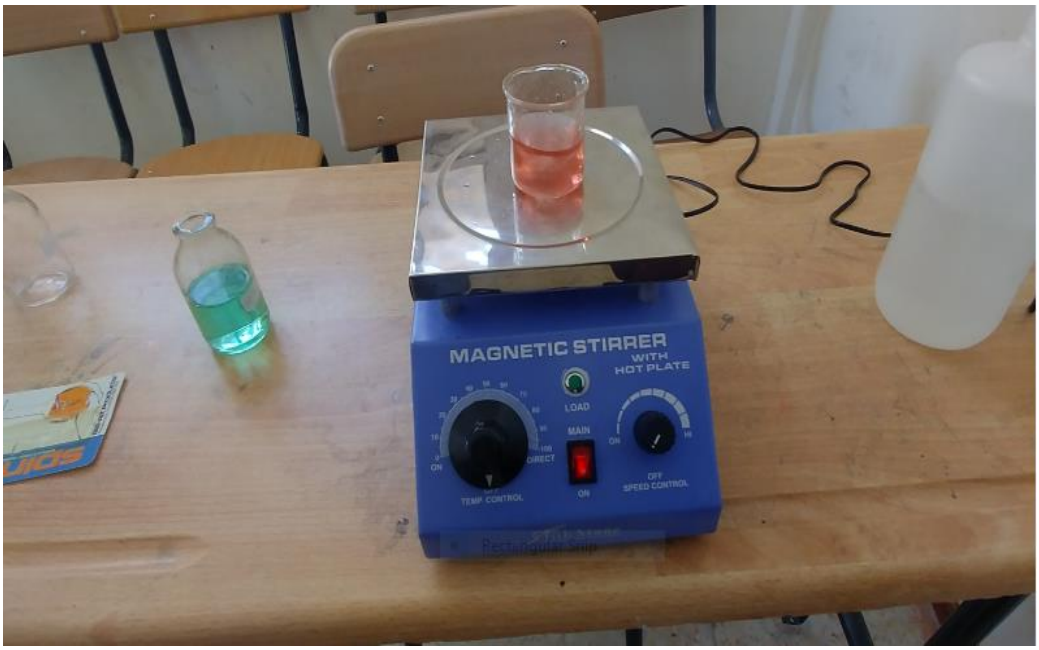

Figure III.6: *The dopant and Stirring process*

III.2.4 Preparation of substrates:

We used glass substrates from the type (CITOPLUS-REF-0302-0004). **(Figure III.7)**

These substrates have been cleaned to ensure the adhesion of the layer. This cleaning is done in several stages:

➢cleaning with laying acid 5 min.

➢a distilled water bath.

➢an alcohol bath (acetone) for 5 min.

➢ drying.

Figure III.7: *The type of substrate used.*

III.2.5 Experimental conditions:

the deposit time: from 35min to 1h45min

- 0% (pure) 35min
- 1%Doped 1h15min
- 3%Doped 40min
- 5%Doped 1h45min

- ❖ the quantity of the solution: 10ml.(4 sample)
- ❖ Concentration of thesolutions: 0,1 mol.l^{-1}
- ❖ the substrate temperature: 400 ° C.(**Figure III.8**)

Figure III.8: *The temperature used to heat the substrate (400 C°)*

- Spout-substrate distance: 10 cm.
- Pressure: 2 bar.(**Figure III.9**)

Figure III.9: *Compressor to raise the required pressure.*

Mass (**Figure III.10**) :

- m(NiO) = 2.9080 g
- m(Co) = 0.5601 g

Figure III.10: Sensitive electrical balanceBP152

The solution was prepared according to the relations:

$$n = C \times V$$

$$n = \frac{m}{M}$$

$$m = M \times C \times V$$

n : *material quantity*

m : *Mass*

M : *Molar mass*

C : *concentration*

V : *the volume*

III.3 Characterization techniques:

The techniques used for the characterization of the thin layers produced are:

- X-ray diffraction (DRX): for the study of structural properties.
- The UV-Visible spectrophotometer: for the study of optical properties.
- The four-point technique: for the study of electrical properties.

III.3.1 Structural characterization:

III.3.1.a *X-ray diffraction (DRX):*

III.3.1.a.A Introduction:

X-ray diffraction crystallography for powder samples is well-established and widely used in the field of materials characterization to obtain information on the atomic scale structure of various substances in a variety of states. Of course, there have been numerous advances in this field, since the discovery of X-ray diffraction from crystals in 1912 by Max von Laue and in 1913 byW.L. Bragg andW.H. Bragg. The origin of crystallography is traced to the study for the external appearance of natural minerals and a large amount of data have been systematized by applying geometry and group theory. Then, crystallography becomes a valuable method for the general consideration of how crystals can be built from small units, corresponding to the infinite repetition of identical structural units in space.[47]

III.3.1.a.B Energy dispersive powder X-Ray Diffraction:

X-Ray diffraction is used for the investigation of crystalline materials. All crystalline materials have one thing in common: their components (atoms, ions or molecules) are arranged in a regular manner. This is a necessary requirement for XRD as diffraction can only occur, if X-rays are scattered by a periodic array of particles with long-range order **(Figure III.12)**.

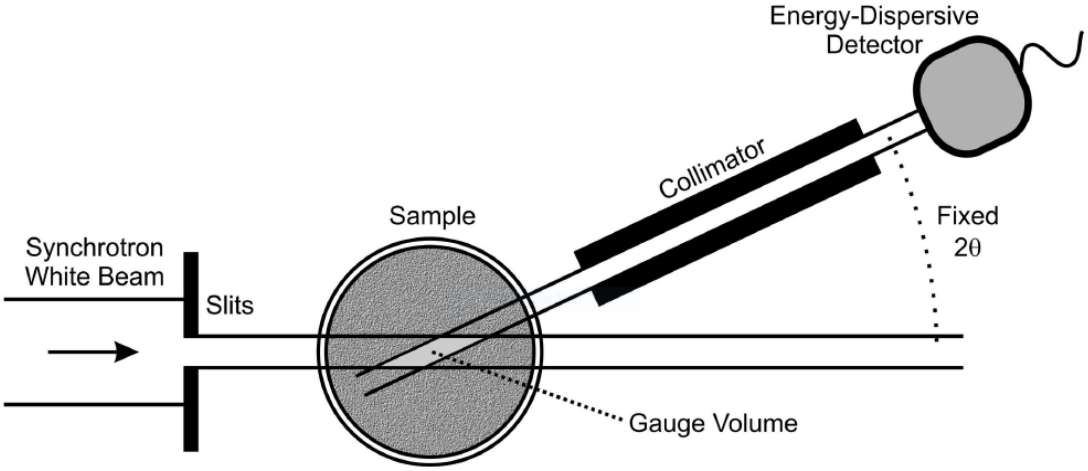

Figure III.12: *Schematic representation of the energy dispersive diffraction (EDD) technique. The energy discriminating detector at fixed scattering angle determines the wavelength of each detected photon and hence the d spacing of the diffracting lattice planes.[48]*

The propagation velocity $\boldsymbol{c}$ of electromagnetic wave (velocity of photon) withfrequency $\boldsymbol{\upsilon}$ and wavelength $\boldsymbol{\lambda}$ is given by the relation:

$$c = v\lambda(ms^{-1}) \qquad \textbf{(III.1)}$$

The velocity of light in the vacuum is a universal constant given as c =299792458 ms^{-1} ($\approx 3 \times 10^{8} m.s^{-1}$). Each photon has an energy E, which isproportional to its frequency,

$$E = hv = \frac{hc}{\lambda} \qquad \textbf{(III.2)}$$

Where h is the Planck constant (6:6260_ 10_34 J _ s).With E expressed in keV, and λ in nm, the following relation is obtained:

$$E(kev) = \frac{1.240}{\lambda(nm)} \qquad \textbf{(III.3)}$$

The momentum p is given by m*v*, the product of the mass m, and its velocity *v*. The de Broglie relation for material wave relates wavelength to momentum.

$$\lambda = \frac{\mathrm{h}}{\mathrm{p}} = \frac{h}{\mathrm{mv}} \qquad \textbf{(III.4)}$$

The resulting diffracted X-rays therefore have a different optical path length to travel. The magnitude of this path length only depends on the distance between the crystal planes and the incident angle of the X-ray beam. This is summarized in the famous Bragg – Equation **(Figure III.13)**:

$$n\ 2\ dsin\theta \quad \textbf{(III.5)}$$

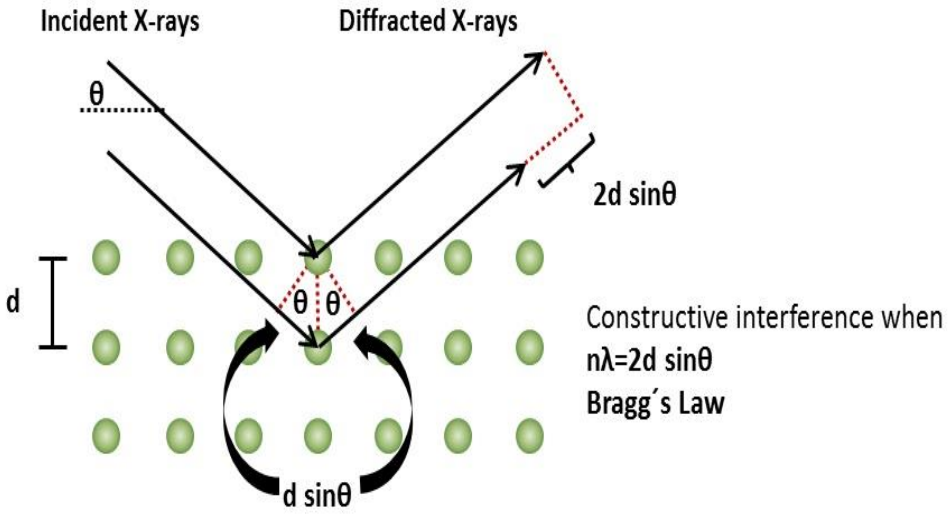

Figure III.13: *Schematic representation of the bragg equation[49]*

III.3.1.a.C Obtainable information from a diffractogramm:

- **Qualitative Analysis:** Every crystalline material produces a specific diffractogramm. This can be seen as the fingerprint of the sample. Comparison of the obtained data with databases results in the identification of the material.
- **Quantitative Analysis:** If the sample is not a pure substance, but consists of several components, it is also possible to calculate the relative amounts of the individual phases.
- **Unit Cell Lattice Parameters:** As mentioned above crystalline materials are regularly arranged. The smallest building block of such a regular arrangement is the unit cell of the material. XRD allows characterizing the dimensions of this unit cell. This can be especially interesting under non-ambient conditions.
- **Crystallite Size and Strain:** The crystallite size of the powder has an influence on the width of the obtained peaks. Crystallites that are smaller than ~120 nm give broader peaks. This can be used to extract information about the size of the crystallites. Microstrain in the sample also results in peak broadening. Also this effect can be quantified by XRD measurements.

III.3.2 Optical characterization:

Thickness is one of the most important thin-film parameters since it largely determines the properties of a film.[50]

III.3.2.a *UV-Visible spectroscopy:*

The functioning of optical measurement devices **(Figure III.14)** is based on the observation of changes and effects produced by the interaction of electromagnetic radiation and matter. From a technical viewpoint this requires the generation of electromagnetic radiation, the modification of its characteristics and the control of its propagation through a given space. Similarly, the "fingerprints" which the material leaves on the radiation need to be producible in an easily understood form**(Figure III.15)**.[51]

Figure III.14: *Experimental UV-visible spectroscopy device used (organic materials laboratory. Echahid Hamma Lakhdar University).[52]*

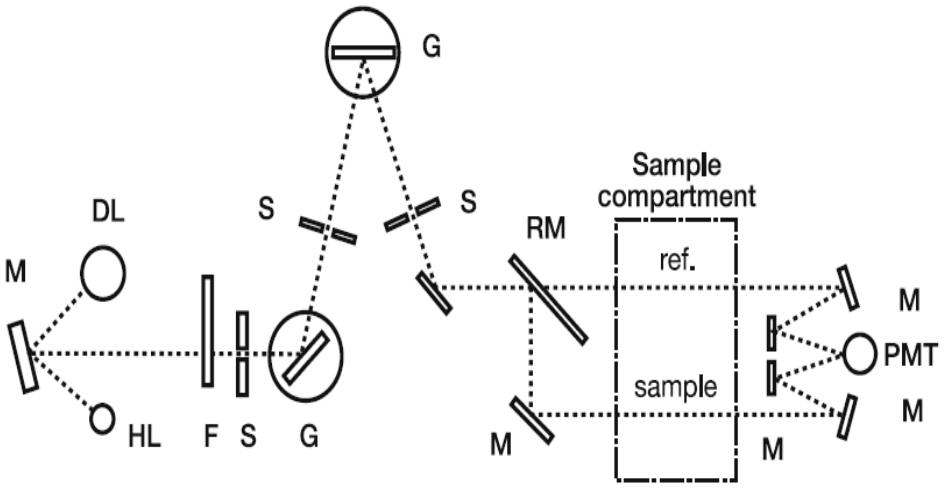

Figure III.15*: The layout of an imaginary spectrophotometer.[53]*

The optical path is indicated by a dotted line.

Components are denoted as follows:

HL = halogen lamp.

DL = deuterium lamp.

M = mirror.

F = filter wheel.

S = slit.

G = grating.

RM = rotating mirror.

PMT = detector (photo multiplier tube).

III.3.2.b *Basic handling of UV spectral:*

The different qualitative methods are presented in (**Figure III.16)**. All these procedures are easy tocarry out either directly with the control software of the spectrophotometer, or with the useof any calculation commercial software (for example, Microsoft Excel).

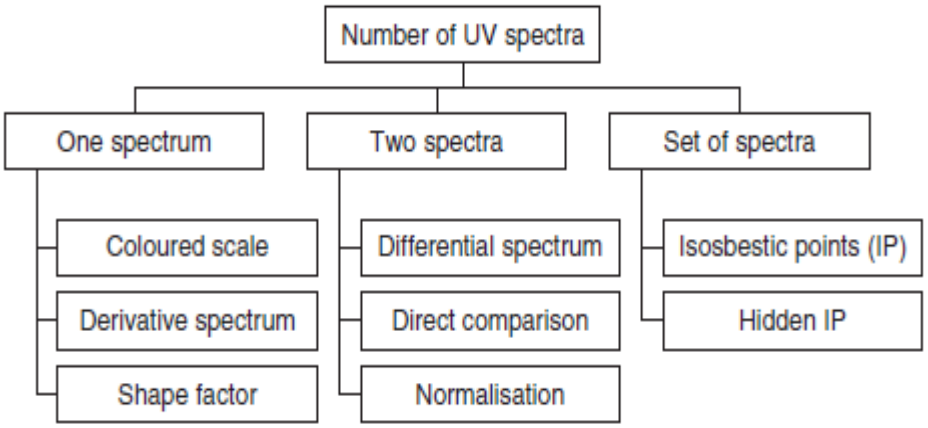

Figure III.16*: Qualitative methods for UV-visible spectra handling[54].*

III.3.2.c *Band gap*

The optical band gap (E_g) of the as-deposited films is determined by the following Tauc relation [55]:

$$\alpha h\nu = A(h\nu - E_g)^n \qquad \textbf{(III.6)}$$

Where:

A is a constant.

$h\nu$ is the incident photon energy.

α is the absorption coefficient.

And n equals to $1/2$ for allowed direct transition.The optical band gap energy value E_g is calculated by extrapolating the linear region of $(\alpha h\nu)^2$ versus $h\nu$ plot[56]

III.3.2.d Urbach tail:

When the doped samples are irradiated with light of a particular wavelength, these defect states trap the excited electrons, preventing their direct transition to the conduction band. Hence, these defect states are responsible for the absorption tail in the absorption spectra[33], which extends into the forbidden gap[57, 58]

This absorption tail is called the Urbach tail and isassociated with the Urbach energy. The equation for calculating the Urbach energy is:

$$\alpha = \alpha_0 + e^{\left(\frac{E}{E_u}\right)} \qquad \textbf{(III.7)}$$

α: is the absorption coefficient.

E : is the photon energy andis equal to hv and E_u is the Urbach energy.[59, 60]

III.3.3 Electrical characterization:

A constant current source injects current through the left outermost probe, which is collected in the right outermost one. The potential difference measured across the inner probes, with a suitably high-impedance voltmeter, is then dependent only on the voltage drop across the specimen surface, eliminating contact resistance phenomena[61].

Figure III.17: Panel (a): Macroscopic probes in which the probe spacing is much larger than the thickness of the surface space–charge layer, and so most of the current passes through the bulk of the crystal.

Figure III.17: Panel (b): Microscopic probes, with schematic illustrations of current paths near a semiconductor surface, penetrating only a distance comparable to the spacing between the probes

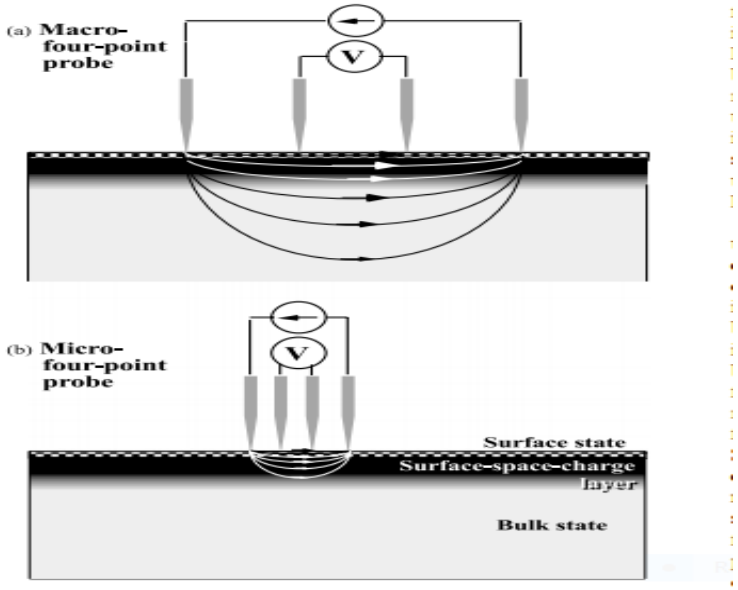

Figure III.17: *Schematic diagram of a linear four-point probe measurement.*

superstructures on the crystal, the measured resistance is normally interpreted as bulk resistance only[61]

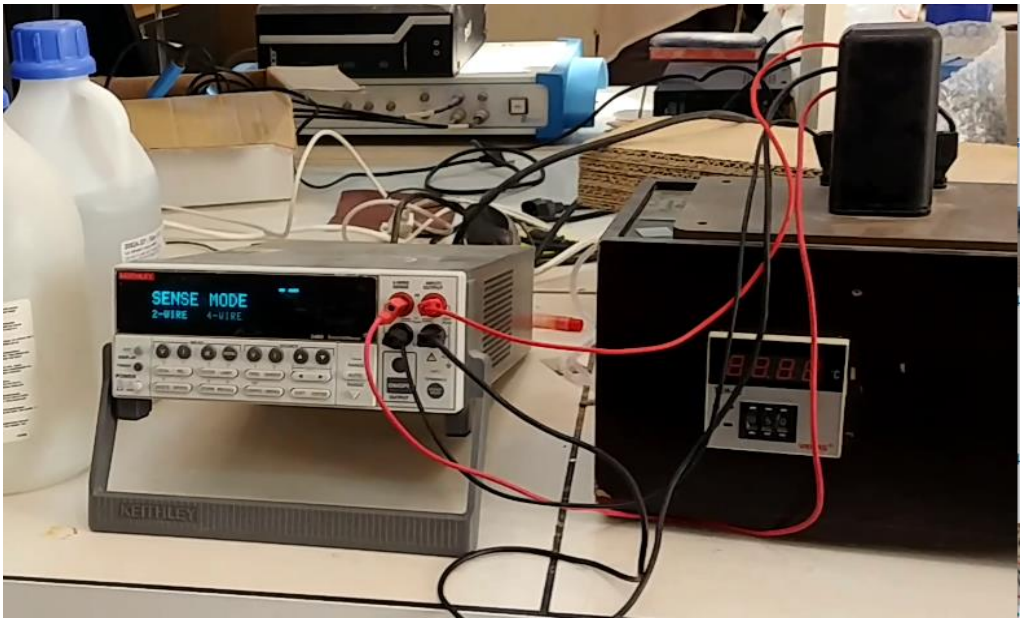

Figure III.18: *Experimental setup of device of the Four-Probe Method used (laboratory, Echahid Hamma Lakhdar University, El Oued).*

III.3.3.a V/I Measurement on a thin layer of thickness e and resistivityρ :

If the thickness is negligible compared to the other dimensions, we can build a two-dimensional model of the conduction which gives:

$$\frac{V}{I} = K \times \frac{\rho}{I} \qquad \textbf{(III.8)}$$

KBeing a dimensionless coefficient characteristic of 2D geometry (shape of contours, position of contacts) **(Figure III.19)**.

The ρ/e ratio characterizes the layer, we denote it byR_S . We then have:

$$\frac{V}{I} = K \times R_S \qquad \textbf{(III.9)}$$

R_S Is expressed in Ohms

The coefficient K can be calculated analytically in a few very simple special cases, for example for 4 spikes aligned equidistant on a limitless layer (infinite):

$$K = \frac{\log(2)}{\Pi} \qquad \textbf{(III.10)}$$

(Practical value:$1/K = 4.532$).

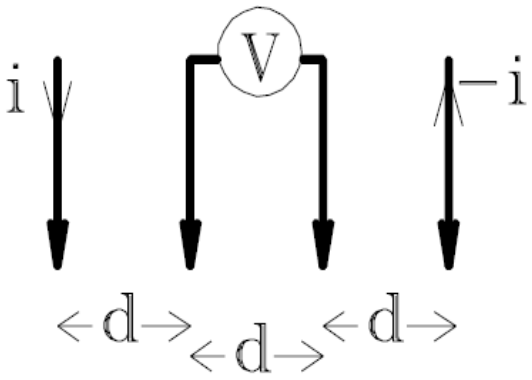

Figure III.19: *K value (special case)*

III.3.3.b Case of a doped layer:

The resistivity is not uniform over the thickness$e$, but formulas (2) and (3) are still applicable, by generalization of the use of R_S. We then define an average resistivity $\rho_m$such that:$R_S = \frac{\rho_m}{e}$

bIf the distribution law of the dopant is known, we can deduce from ρ_m the surface concentration and for different depths (see charts).

III.3.3.c Practical method for 4-point measurement:

• perform a $^V/_I$ measurement not too close to the edges of the sample.

• express the measurement in $Ohms$.

• multiply by 4.532 to obtain R_S, note this result (always in $Ohms$)(the distance between centers being 1.59 mm, the thickness correction is not necessary).

• express the thickness e of the layer in cm.

• multiply R_S by e to obtain the resistivity ρ or ρ_m , note this result (in $Ohm.cm$).

• use an abacus to deduce the dopant concentration (after possibly conductivity calculation in$\mathrm{Ohm}^{-1}.Cm^{-1}$).

BE CAREFUL: it is not the same chart according to whether the doping is uniform (substrate,

Polysilicon deposited) or not (diffused or implanted layer).

III.4 Conclusion:

In this chapter, we have described the different characterization techniques used to analyze and determine the different structural, optical and electrical properties of the thin layers of pure and cobalt-doped NiO nanostructures produced.

IV Chapter IV:

Results and discussion

IV.1 Introduction:

In this chapter we have explained the various experimental results obtained (structural, optical and electrical properties) on the thin layers of pure and cobalt-doped nickel oxide and the discussion.

IV.2 Thin Films Characterization.

IV.2.1 Results and discussion

Structural characterizations are carried out using X-ray diffraction (XRD) with an X-ray diffractometer (BRUKER-AXS type D8) equipped with X'Pert High Score under Cu Kα (λ =1.5406 Å) radiation, whereas the scanning range of (2θ) was between 20° and 70°, Optical transmittance of the deposited thin films was measured in the range of 300–900 nm by using an UV-visible spectrophotometer (SHUMATZU 1800). To affirm the p-type conductivity and its variation with precursor concentration, Seebek effect and four-point probe were processed on sheets having $1cm^2$ for all the samples.

IV.2.1.a *Structural characterization:*

(Figure 1) shows the X-ray spectrum of the thin-films of pure nickel oxide and cobalt doped at different percentage (1%, 3%, 5%), developed at a temperature of 400°C

Figure.IV.1: *X-ray diffraction spectra of pure NiO and Co-doped NiO thin films*.

The X-ray diffraction patterns of the as-fabricated films on the glass substrates. From the literatures (Joint Committee on Powder Diffraction Standards (JCPDS) **(Figure.IV.2)** card No. 47-1049), all the diffraction peaks of the films match with the NiO face-centered cubic (fcc) structure. The peaks at scattering angles (two theta) of 37.48°, 43.47°correspond to crystal planes of (111), (200) of crystalline NiO, respectively, from this XRD patterns, no other impurity peaks, were detected, indicating that no other products existed in as-fabricated NiO films. The thin film that can be seen, deposited at all patterns, has a higher (43.47°) and sharper (200) diffraction peak indicating an improvement in the crystallization of films. The positions of the peaks and the presence of more than one diffraction peak lead to the conclusion that the films are polycrystalline in nature with a cubic crystalline structure. In order to obtain more structural information, different structural parameters such as lattice constants$a$, interplanar

spacing d_{hkl} , grain size$D$, mean strain ε, and dislocation density δ of NiO thin films coated on various precursor concentration are calculated. In the case of cubic structure.

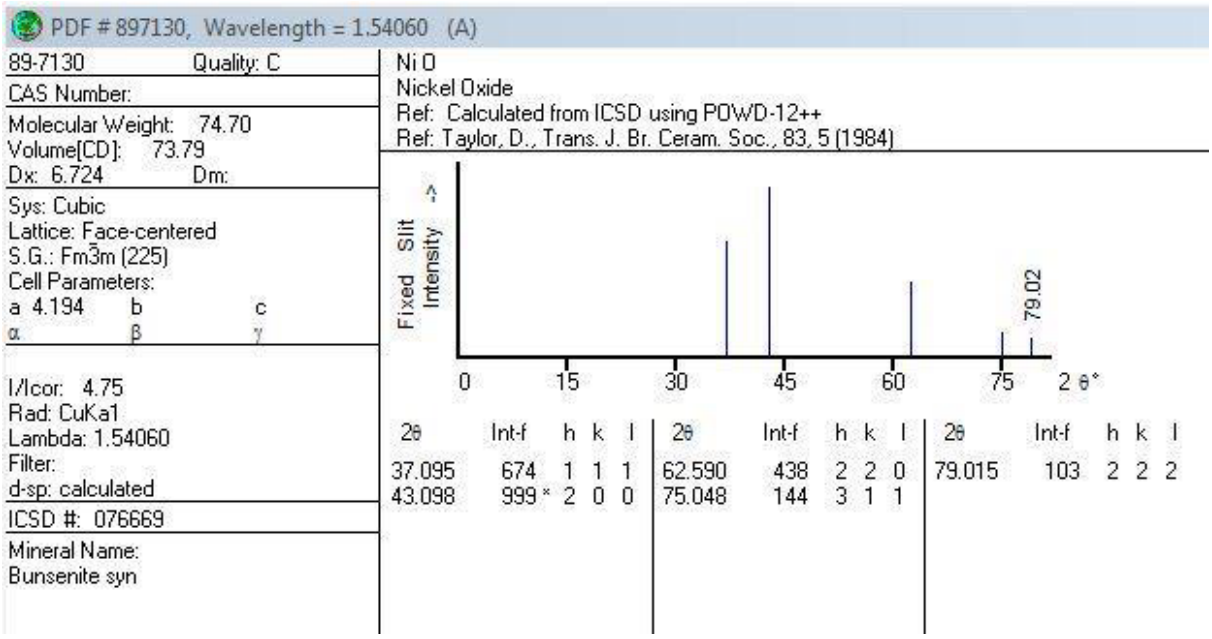

Figure.IV.2: *Card JCPDS N ° 47-1049, de NiO.[18]*

The lattice constant a for NiO a phase is calculated using the following equation[62]:

$$d_{hkl} = \frac{a^2}{\sqrt{h^2+k^2+l^2}} \qquad \textbf{(IV 1)}$$

Where hkl are Miller indices and d_{hkl} is the interreticular spacing given by Bragg's law:[63]

$$2d_{hkl}sin\theta = n\lambda \qquad \textbf{(IV 2)}$$

Where n is the diffraction order taken equal to unity (first order), λ is the wavelength of the radiation (λ = 1.540593 Å) for the CuKa radiation and θ is the Bragg diffraction angle of peak in radian.The grain size D of the films was calculated for the (111) plane using Scherrer's equation:[64]

$$D = \frac{0.9\lambda}{\beta\ cos\ \theta_{hkl}} \qquad \textbf{(IV 3)}$$

Where β the full width at half maximum (FWHM) corresponding to the diffraction angle and λ is the X-ray wavelength of the incident radiation (1.540593 Å).

The mean strain ε in NiO thin films can be estimated using the formula:[65]

$$\varepsilon = \frac{a-a_0}{a_0} \times 100\% \qquad \textbf{(IV 4)}$$

Where a and a_0 are the NiO thin film lattice constants and the standard lattice constant of the bulk material (= 4.1769 Å)

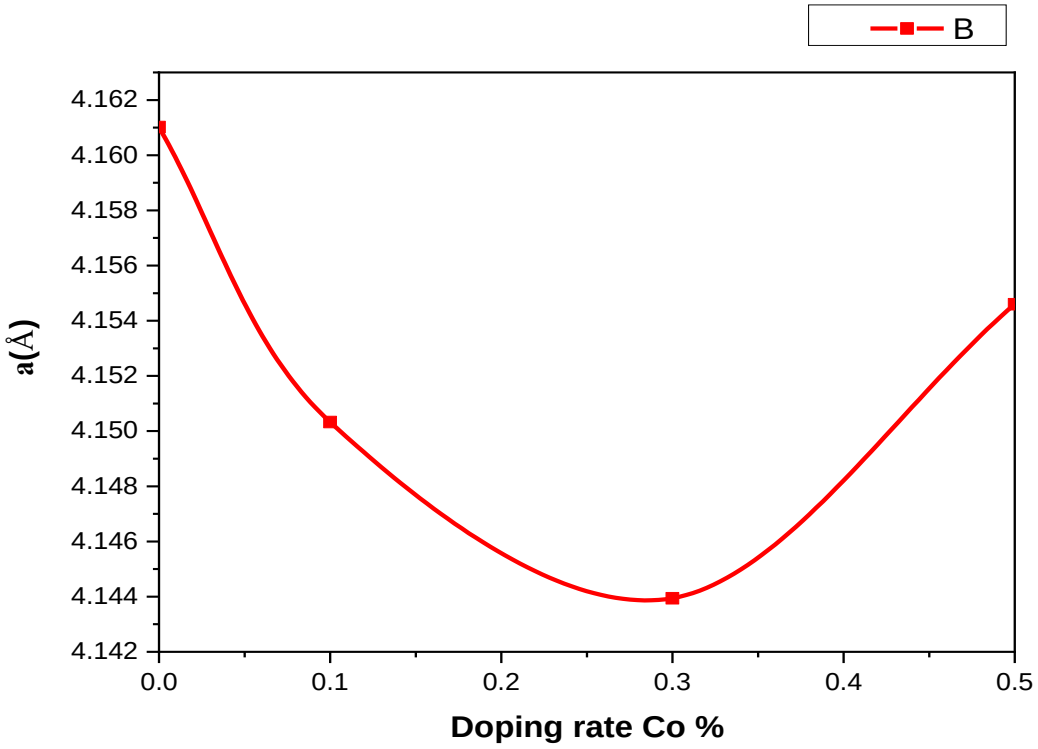

Figure.IV.3: *Variations of the lattice constant (a_0) of NiO thin films as function of Co doping concentration at 400° C.*

It can be noticed that the lattice constant (a_0) decreases rapidly as the Co-concentration increases from 0 to 3% and then increases as the 5% further to reach value of (14.15 Å) as shown in (**Figure 2).** It should be mentioned here that the standard $a_0$value for NiO (4.176Å) according to the standard card (JCPDS, No 47-1049), which indicates that the undoped NiO film has the nearest a_0 value to the standard lattice constant (4.16Å).

The dislocation density δ, which is defined as the dislocation line per unit volume, has been calculated using the following relation:[66]

$$\delta = \frac{1}{D^2} \qquad \textbf{(IV 5)}$$

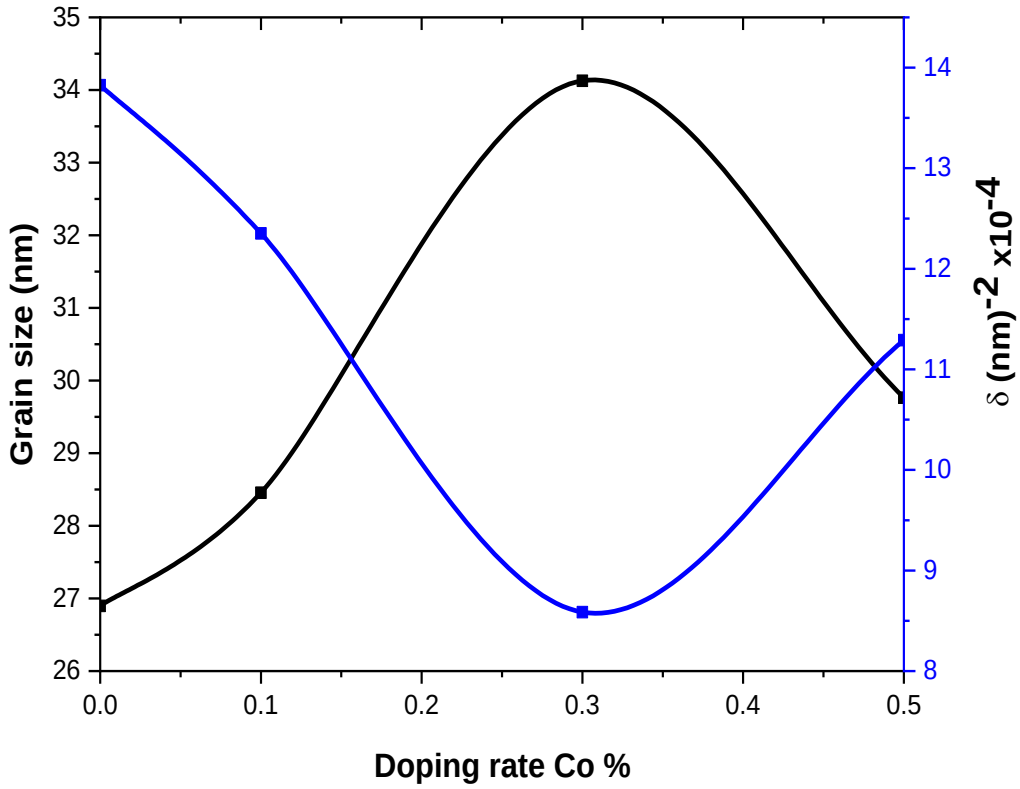

Figure.IV.4: *Variations of grain size and dislocation (ε) of NiO thin films as function of Co doping concentration at 400° C.*

In **(Figure 4)**. As can be seen from this figure when the Co concentration covers the average 0–5%, the grain sizes of the thin films were about 26.89, 28.45, 34.12, and 29.76 nm for samples deposited using 0%, 1%, 3%, and 5%, respectively. The film prepared at 3% the high value of grain size (34.12 nm) revealing the nanostructure of the product. The increase in the grain size indicates a decrease in the lattice defects and vice versa, which in turn reduces internal strain and dislocation density as it was seen in **(TableIV1)**.

(Table IV1) summarizes variations of different structural parameters of elaborated NiO and Co doped thin films with various concentrations. Variation of grain size along the (111) plan as a function of Co doping concentration is reported

TableIV.1: *Values of Bragg angle 2θ, lattice constants a, full width at half maximum β, grain size D, mean strain ε, and dislocation density δ deduced from the (111) peak of NiO and cobalt doped prepared at 400° C with different concentration..*

Co (%)	2θ	hkl	(β°)	D (nm)	ε (%)	δ $(nm)^{-2}$ x 10^{-4}	α (Å)
0	**37.438**	**111**	**0.312**	**26.8952**	**-2.2727**	**13.8245**	**4.1610**
1	**37.572**	**111**	**0.295**	**28.4535**	**-0.5289**	**12.3517**	**4.1503**
3	**37.572**	**111**	**0.246**	**34.1272**	**-0.6821**	**8.5862**	**4.1439**
5	**37.505**	**111**	**0.282**	**29.7617**	**-0.4266**	**11.2897**	**4.1546**

And

θ: Bragg angle values

ε: Mean strain

δ: Dislocation density

β: The total width at half height

D: Grain size

IV.2.1.b *Optical analysis :*

Optical transmittance spectra of the films in spectral range of (300-900 nm) were recorded by using UV–visible spectrophotometer. **(Figure IV 5)** shows the relation between transmittance and wavelength for Co-doped Nickel Oxide thin films. For all thin films prepared at various precursor concentrations, spectra show two regions:

The first one at wavelength higher than 400 nm showing practically an average transmission between 38.17 and 64.66% and revealing a decrease by increasing the Co doping concentration

and, based on calculated film thickness (t), transparence was found to be depending on thickness of samples reveling Beer-Lambert low as it was shown in (**Table IV2).**

The second region is at wavelength lower than 400 nm for which transparence decreases rapidly for all samples exhibiting the onset fundamental absorption due to the transition between the valence band and the conduction band.

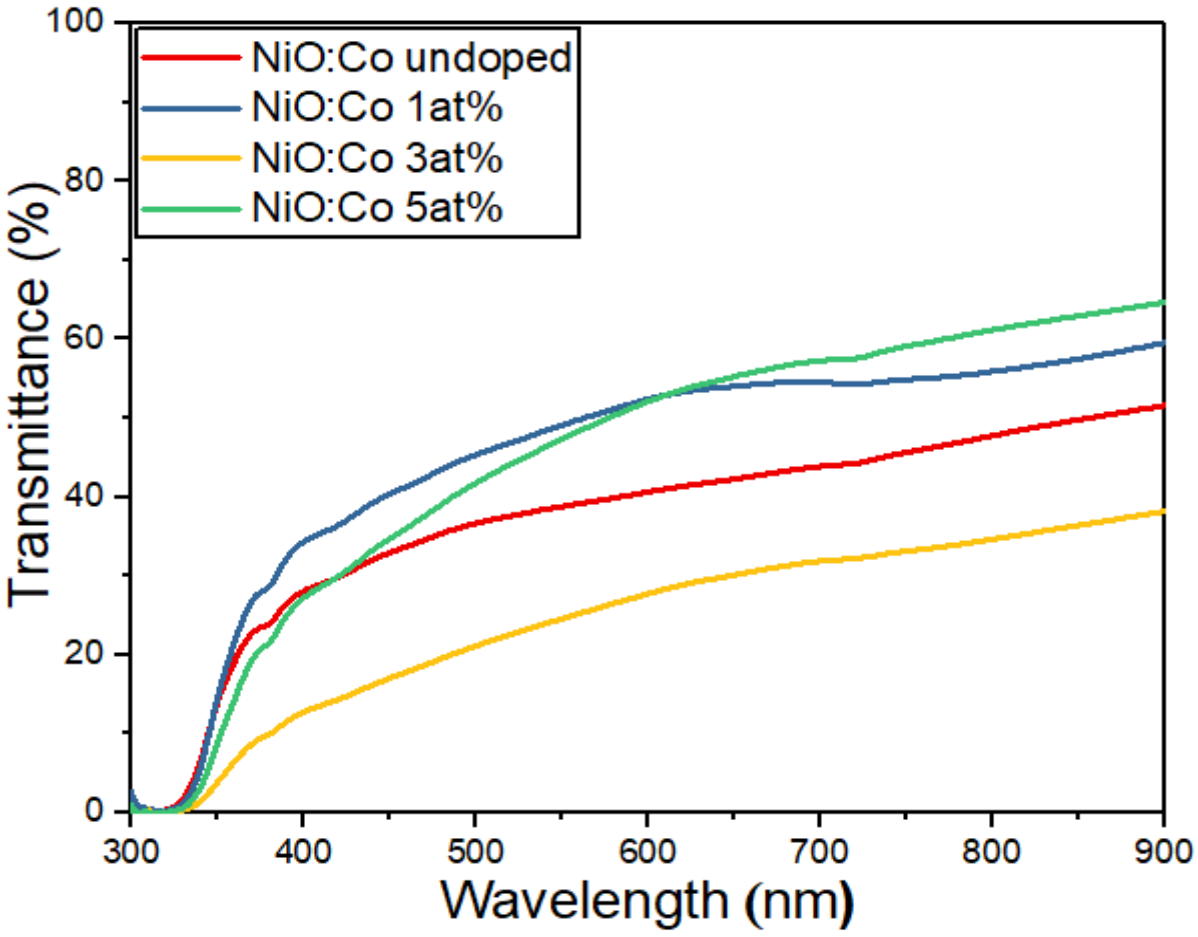

Figure.IV.5: *spectral transmittance plots of NiO thin films prepared at 400°C with different Co doping concentration.*

***TableIV.2**: Values of thickness t, average transmittance, optical band gap energy E_g , and Urbach energy E_u of NiO thin films prepared at 400°C with different of Co doping concentration .*

Co (%)	**Thickness t (nm)**	**Average transmittance (%)**	**Gap energy Eg (eV)**	**Urbach energy Eu (MeV)**
0	402	51.55	3.60	293
1	345	59.54	3.58	241
3	475	38.17	3.47	285
5	352	64.66	3.55	279

For more investigation, absorption coefficient (α) of the NiO thin films was determined from the transmittance measurements using Swanepoel's method[67, 68]:

$$\alpha = \frac{1}{t}\ln(\frac{1}{T}) \qquad \textbf{(IV 6)}$$

Where t and T are the thickness and transmittance of the film, respectively. Energy gap values depend in general on the films crystal structure (disorder and its regularity)[69]. Also (α) and the incident photon energy (h) are related each other as they are given in Tauc equation:[70]

$$\alpha h\nu = A(h\nu - E_g)^n \qquad \textbf{(IV 7)}$$

where A is a constant, Eg is the band gap of the material, and n is an exponent which depends on the type of transition; n = 1/2; 2; 3/2; and 3 correspond to allowed direct, allowed indirect, forbidden direct, and forbidden indirect, respectively. Direct energy gap was determined by plotting a graph between $\alpha h\nu^2$ versus $h\nu$ and extrapolation of straight line to $\alpha h\nu^2 = 0$ gives the direct band gap values of different concentrated sprayed NiO thin films as seen in Figure 3

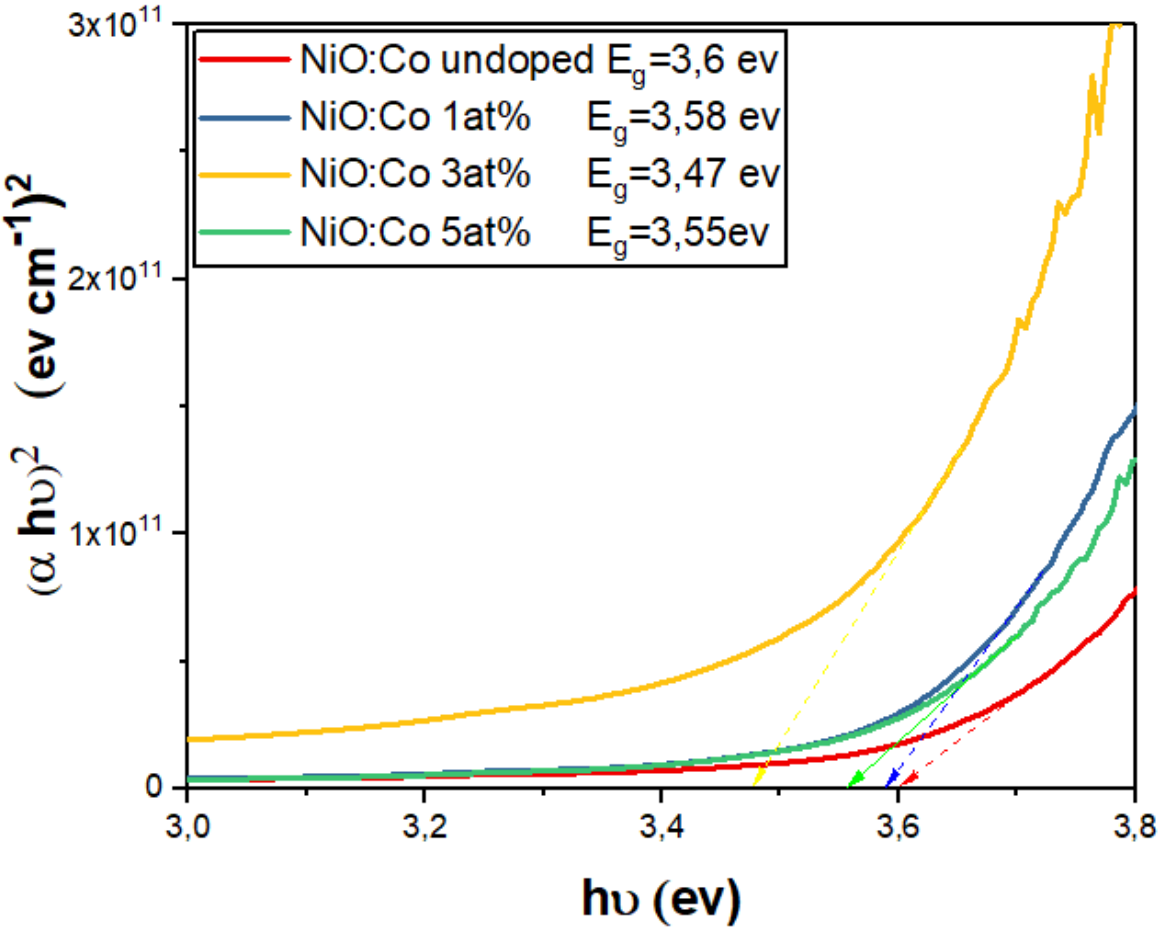

Figure .IV.6: *Band gap (E_g) estimation from Tauc's relation of pure NiO and Co-doped NiO thin at 400°C with different of Co doping concentration*

The calculated band gap values are listed in (**Table IV2)**. Obtained band gap values are in good agreement with results carried out in literature[71, 72]. A disorder, so called Urbach tails, which is related to width of the localized states available in the optical band gap of the NiO thin films and affected its structure, was done for further investigation. This width, of the localized states, is related directly to a similar exponential tail for the density of states near band edges and can be expressed by the following relation[73]:

$$\alpha = \alpha_0 \exp(\frac{hv}{E_u}) \qquad \textbf{(IV 8)}$$

Where hv is the photon energy, α_0 is constant, and E_u is the Urbach energy which refers to the width of the exponential absorption edge.

(Figure IV 7) shows the variation of versus photon energy (hv) for the films. Values were calculated from reciprocal of the straight line slopes, as shown in the **(Figure IV7)**, and illustrated in **(Table IV2)**. As can be seen from **(Table IV2)**, the energy band gap is averaged in (3.47 – 3.60 eV). The decrease in the optical band gap with Co doping concentration may be

attributed to the increase in grain size and decrease in structural disorder in the films as observed from Urbach energy analysis.

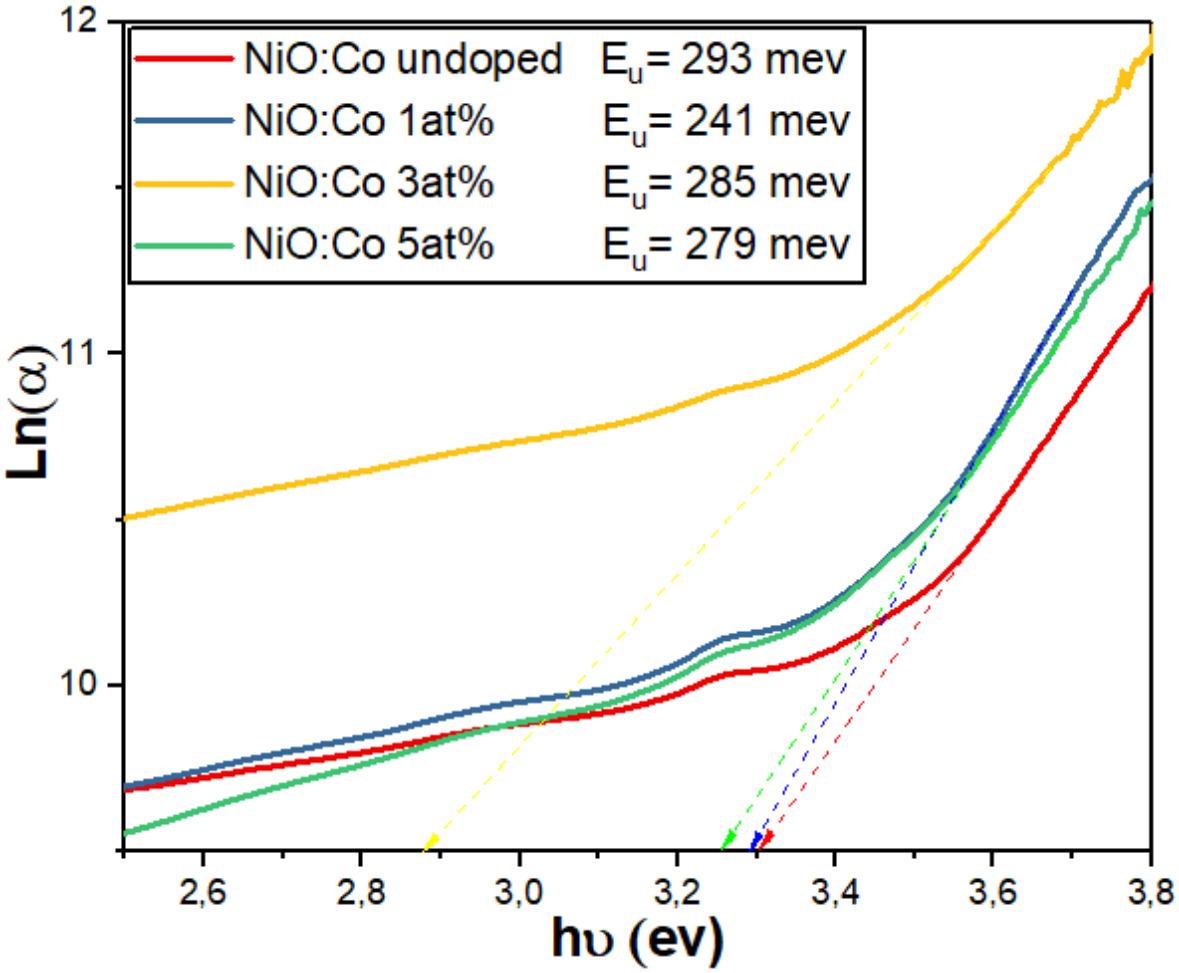

Figure.IV.7: *Variation of band gap (Eg) and Urbach energy (Eu) of NiO thin films as function of Co doping concentration of pure NiO and Co-doped NiO thin films prepared at 400 °C*

.In **(Figure IV8)** a comparison is given between the variations of the optical gap and the energy of the thin films as a function of Co doping concentration. Generally, we notice that the two preceding parameters are varied inversely according to Co-concentration. The decrease in the energy value of Urbach indicates that the film has fewer defects and therefore an increase in the optical gap and this gives us a good transparency of the film and vice versa.

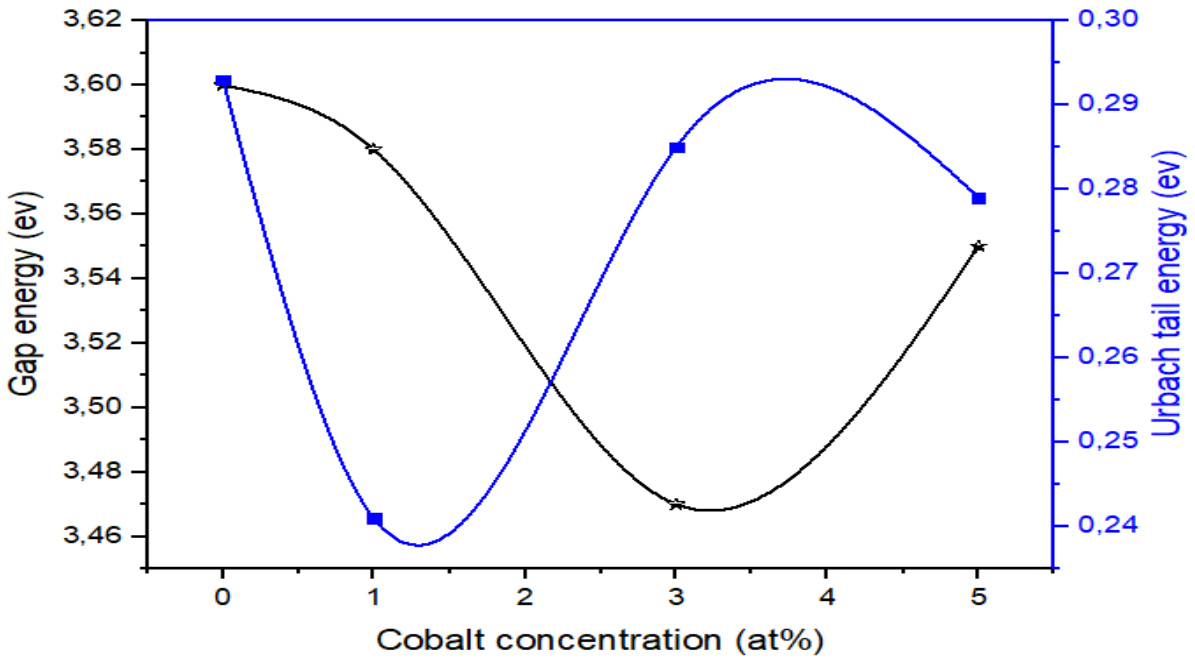

Figure.IV.8: *Comparison of optical gap values with Urbach energy values of Co doping concentration*

IV.2.1.c *Electrical Properties:*

The resistance (Rs) was measured using the four-point technique, from the voltage (V) and current intensity (I) values found experimentally.

Conductivity is considered to be one of the electrical more important. It can be calculated from the values of the resistance (Rs) and the thickness (d) using the following formula:

$$\sigma = \frac{1}{R_s \times d} \qquad \textbf{(IV 9)}$$

Table *IV*.4*: Results of measurements obtained from Rs and σ.***

Co (%)	$R_s.10^5$ (Ω)	$\sigma.10^{-8}(\Omega.cm)^{-1}$
0	9.7	0.25
1	4.89	0.57
3	8.05	0.26
5	6.55	0.43

It is worth noting that NiO is known as a p-type semiconductor due to the Ni+2 vacancies which is the considered defect for its p-type conductivity [74, 75]. Seebek effect was processed on all the samples and confirmed their p-type conductivity. As can be seen from this table the conductivity of the NiO thin films increases from $0.25\Omega^{-1}\ cm^{-1}$) for thin film deposited with 0 Co (%) to a value ($0.57\Omega^{-1}\ cm^{-1}$) at 1 Co (%) then decreases to reach $0.26\ \Omega^{-1}\ cm^{-1}$ at 3 Co (%). and then increase again to reach $0.43\Omega^{-1}\ cm^{-1}$) at 5 Co (%). The electrical conductivity (σ) was correlated to the film thicknesses revealing the same behavior upon the Co doping concentration.

IV.3 Conclusion:

In this chapter, we elaborated the NiO thin films, then we studied the effect of nickel oxide doping with cobalt on structural properties, optical properties and electrical properties of. The XRD patterns showed that the structure of the undoped and doped NiO films is polycrystalline structure with the preferred direction (111),(200) respectively also showed that there was no significant shift in the direction of diffraction peaks after doping with cobalt. The crystalline size is increased by increasing the doping in the (NiO) samples. From the transmittance spectra, for all samples it was observed that the optical transparency values were averaged, it increase by increasing the percentage of doping with cobalt and it decreased at (3%) This may be due to inappropriate experiment conditions, Cobalt doping was also found to be increasing the band gap energy, and its values ranged from 3.47 to 3.60 eV. It was observed that the electrical conductivity of all samples is good and it is the P-type, and the best conductivity has been obtained for the nickel oxide layer doped with 1% cobalt ($0.57 \times 10^{-8}\ (\Omega.cm)^{-1}$).

General conclusion

General conclusion

This work has been based on the chemical spray pyrolysis technique by exploiting solar energy as a source of heat, and this method is considered the most effective, that for its ease and low cost on the one hand and the quality of the films prepared by it on the other hand, it is used to produce thin films for different applications including the most important (TCO). In this work, we prepared and characterized samples of the thin films of nickel oxide, which were doped with different percentages of cobalt (0%, 1%, 3%, 5%), where we deposited these layers on glass substrates.

The aim of this work is to study the effect of nickel oxide doping with cobalt on structural properties, optical properties and electrical properties, by using the solar energy for generate the heat to operate on the deposition of nickel on a glass substrate.

To characterize these samples, we used several techniques, such as X-ray diffraction for structural characterization, UV-Visible spectroscopy for optical characterization and the four-point method for electrical characterization

The spectra obtained by X-ray diffraction showed that the structure of the thin films of cobalt-doped nickel oxide that we developed is a crystalline structure; the peaks appear at $2\theta \approx 37°$, $2\theta \approx 44°$ with a preferential orientation according to the planes (111),(200) respectively which indicates that these layers crystallize in the cubic structure

The results obtained by the analysis by UV-Visible spectroscopy have allowed us to determine some optical properties such as, the transmittance between 38.17 and 64.66% in the visible range and the infrared, which proves that the layer transmits light in these areas. The energy values of the optical gap vary between 3.47 eV and 3.60 eV and the smallest value, which is 3.47 eV, was found for the doping at 3%. Urbach's energy varies inversely with that of the gap; it is between 241MeV and 293 MeV.

Regarding the electrical properties, the results obtained by the four-point method show us that the best conductivity is that which was obtained for the layer of nickel oxide doped with 1% cobalt, it is of the order of$0.57 \times 10^{-8}(\Omega.cm)^{-1}$, the other values of the conductivity, for the other percentages of cobalt, are between $0.25 \times 10^{-8}$and$0.57 \times 10^{-8}\ (\Omega.cm)^{-1}$, and the best conductivity has been obtained for the nickel oxide layer doped with 1% cobalt

References :

[1] Y. Benkhetta, "L'effet du débit de la solution sur les propriétés des couches minces d'oxyde de zinc (ZnO) déposées par spray ultrasonique," 2013.

[2] B. D. Berrouis Soumia, "Elaboration et caractérisation de couche mince NiO: Co."

[3] L. Smaoun, C. Bellagh, and N. Ait Ahmed, "Électrodéposition des couches minces de l'oxyde de nickel et étude de leur activité électro catalytique vis-à-vis de l'oxydation du Méthanol et du Propanol," Université Abderrahmane Mira-Bejaia, 2016.

[4] A. A. Iyanda and C. I. J. I. Iheakanwa, "Tissue histology and antioxidant defense system in female rats exposed to sun rays," vol. 4, pp. 5-8, 2014.

[5] A. Messai, Y. Benkedda, S. Bouaichaoui, and M. J. E. P. Benzerga, "Feasibility study of parabolic trough solar power plant under Algerian climate," vol. 42, pp. 73-82, 2013.

[6] P. Singhal, "A Case Study on Energy Efficient Green Building with New Intelligent Techniques Used to Achieve Sustainable Development Goal," in *2019 20th International Conference on Intelligent System Application to Power Systems (ISAP)*, 2019, pp. 1-7: IEEE.

[7] J. Pérez Caballero, "Comparision between PV and CSP plants through LCA aproach," 2012.

[8] Q. Sylvain, "Les centrales solaires a concentration," *Université de Liège*, p. 4, 2007.

[9] R. Muthusivagami, R. Velraj, R. J. R. Sethumadhavan, and S. E. Reviews, "Solar cookers with and without thermal storage—a review," vol. 14, no. 2, pp. 691-701, 2010.

[10] V. Lemmer, "Comparative market analysis and economic simulation for Morocco of the parabolic trough and dish CSP technologies," 2014.

[11] A. Hafez, A. Soliman, K. El-Metwally, I. J. E. C. Ismail, and Management, "Solar parabolic dish Stirling engine system design, simulation, and thermal analysis," vol. 126, pp. 60-75, 2016.

[12] A. A. Badran *et al.*, "Portable solar cooker and water heater," vol. 51, no. 8, pp. 1605-1609, 2010.

[13] G. Rajamohan, P. Kumar, M. Anwar, and T. Mohanraj, "Analysis of solar water heater with parabolic dish concentrator and conical absorber," in *IOP conference series: materials science and engineering*, 2017, vol. 206, no. 1, p. 012030: IOP Publishing.

[14] G. Rajamohan, P. Kumar, M. Anwar, and T. Mohanraj, "Analysis of solar water heater with parabolic dish concentrator and conical absorber," in *IOP conference series: materials science and engineering*, 2017, vol. 206.

[15] L. Schaper, D. J. I. t. o. c. Amey, hybrids,, and m. technology, "Improved electrical performance required for future MOS packaging," vol. 6, no. 3, pp. 283-289, 1983.

[16] N. N. Greenwood and A. Earnshaw, *Chemistry of the Elements*. Elsevier, 2012.

[17] D. G. J. U. s. E. o. I. C. Kerfoot, "Nickel," 2000.

[18] M. Ghougali, "Elaboration and characterization of nanostructuring NiO thin films for gas sensing applications," University of Mohamed Khider, BISKRA, 2019.

[19] I. E. Britannica, *Encyclopaedia britannica*. Encyclopaedia Britannica, Incorporated, 1957.

[20] N. Greenwood and A. Earnshaw, *Chemistry of the Elements 2nd Edition*. Butterworth-Heinemann, 1997.

[21] E. Thimsen, A. B. Martinson, J. W. Elam, and M. J. Pellin, "Energy levels, electronic properties, and rectification in ultrathin p-NiO films synthesized by atomic layer deposition," *The Journal of Physical Chemistry C,* vol. 116, no. 32, pp. 16830-16840, 2012.

[22] R. Sanderson, "Chemical Periodicity, Reinhold Pub," *Corp., New York,* p. 24, 1960.

[23] F. Si, F. Tang, and H. Xue, "Electronic properties of NiO (1 1 0)/CH3NH3PbI3 (1 0 0) interface from the first-principles calculations," *Chemical Physics Letters,* vol. 707, pp. 133-139, 2018.

[24] S. Van Houten, "Semiconduction in LixNi1− xO," *Journal of Physics and Chemistry of Solids,* vol. 17, no. 1-2, pp. 7-17, 1960.

[25] S. Houten, "Semiconduction in LixNi (1-x) O," *J. Phys. Chem. Solids,* vol. 17, p. 7, 1960.

[26] M. Nachman, L. Cojocaru, and L. Ribco, "Electrical properties of non-stoichiometric nickel oxide," *physica status solidi (b),* vol. 8, no. 3, pp. 773-783, 1965.

[27] S. Kakumanu, *Synthesis, Structure and Catalytic Application of Silver (I) Coordination Polymers Based on 1, 2, 4, 5-Tetra (Isopropylthio) Benzene Ligand*. Lamar University-Beaumont, 2017.

[28] R. Powell and W. Spicer, "Optical properties of NiO and CoO," *Physical Review B,* vol. 2, no. 6, p. 2182, 1970.

[29] C. A. Ross, "Patterned magnetic recording media," *Annual Review of Materials Research,* vol. 31, no. 1, pp. 203-235, 2001.

[30] K. Maaz *et al.*, "Effect of crystallographic texture on magnetic characteristics of cobalt nanowires," *Nanoscale research letters,* vol. 5, no. 7, pp. 1111-1117, 2010.

[31] F. Cotton, G. Wilkinson, C. Murillo, and M. Bochmann, "Advanced Inorganic Chemistry, John Willey & Sons," *Inc., New York,* p. 869, 1999.

[32] R. Sanderson and I. Chemists, "Reinhold,“," *Chemical Periodicity", New York, USA,* 1960.

[33] V. Akshay, B. Arun, G. Mandal, and M. Vasundhara, "Visible range optical absorption, Urbach energy estimation and paramagnetic response in Cr-doped TiO 2 nanocrystals derived by a sol–gel method," *Physical Chemistry Chemical Physics,* vol. 21, no. 24, pp. 12991-13004, 2019.

[34] A. Brenner, *Electrodeposition of Alloys: Practical and specific information*. Academic Press, 1963.

[35] H. Amani Hamedani, "Investigation of deposition parameters in ultrasonic spray pyrolysis for fabrication of solid oxide fuel cell cathode," Georgia Institute of Technology, 2008.

[36] D. M. Mattox, "Physical vapor deposition (PVD) processes," *Metal Finishing,* vol. 100, pp. 394-408, 2002.

[37] X.-T. Yan and Y. Xu, *Chemical vapour deposition: an integrated engineering design for advanced materials*. Springer Science & Business Media, 2010.

[38] H. O. Pierson, *Handbook of chemical vapor deposition: principles, technology and applications*. William Andrew, 1999.

[39] J. Creighton and P. Ho, "Introduction to chemical vapor deposition (CVD)," *Chemical vapor deposition*, vol. 2, pp. 1-22, 2001.

[40] A. Hunt, W. Carter, and J. Cochran Jr, "Combustion chemical vapor deposition: A novel thin-film deposition technique," *Applied Physics Letters*, vol. 63, no. 2, pp. 266-268, 1993.

[41] Y. Xu and X.-T. Yan, "Introduction to chemical vapour deposition," *Chemical Vapour Deposition: An Integrated Engineering Design for Advanced Materials*, pp. 1-28, 2010.

[42] A. Ashour, M. Kaid, N. El-Sayed, and A. Ibrahim, "Physical properties of ZnO thin films deposited by spray pyrolysis technique," *Applied Surface Science*, vol. 252, no. 22, pp. 7844-7848, 2006.

[43] G. Korotcenkov, V. Brinzari, J. Schwank, M. DiBattista, and A. Vasiliev, "Peculiarities of SnO2 thin film deposition by spray pyrolysis for gas sensor application," *Sensors and Actuators B: Chemical*, vol. 77, no. 1-2, pp. 244-252, 2001.

[44] I. W. Lenggoro, Y. C. Kang, T. Komiya, K. Okuyama, and N. Tohge, "Formation of submicron copper sulfide particles using spray pyrolysis method," *Japanese journal of applied physics*, vol. 37, no. 3A, p. L288, 1998.

[45] D. Vaufrey, "Réalistion d'OLED à émission par la surface: optimisation de structures ITO/semiconducteurs organiques," Ecully, Ecole centrale de Lyon, 2003.

[46] Y. AOUN, "Conception et développement d'un four solaire pour l'élaboration des oxydes métalliques-caractérisation des oxydes," Université Mohamed Khider-Biskra, 2016.

[47] Y. Waseda, E. Matsubara, and K. Shinoda, *X-ray diffraction crystallography: introduction, examples and solved problems*. Springer Science & Business Media, 2011.

[48] A. Le Bail *et al.*, *Powder diffraction: theory and practice*. Royal society of chemistry, 2008.

[49] L. V. Azároff, R. Kaplow, N. Kato, R. J. Weiss, A. Wilson, and R. Young, *X-ray Diffraction* (no. 1). McGraw-Hill New York, 1974.

[50] L. Eckertová, "Thin Film Thickness and Deposition Rate Measurement Methods," in *Physics of Thin Films*: Springer, 1977, pp. 52-71.

[51] K. Sakoda, *Optical properties of photonic crystals*. Springer Science & Business Media, 2004.

[52] حمد. ت, الباقي. ع, نيد, رياض, فار, and كمال, "L'effet de la molarité de nickel sur les propriétés des couches minces d'oxyde de nickel NiO élaborées par la technique de spray pyrolyse alimentée par énergie solaire," 2019.

[53] J. A. Räty, K.-E. Peiponen, and T. Asakura, *UV-visible reflection spectroscopy of liquids*. Springer Science & Business Media, 2004.

[54] O. Thomas and C. Burgess, *UV-visible Spectrophotometry of Water and Wastewater*. Elsevier, 2017.

[55] O. Shevaleevskiy, "The future of solar photovoltaics: A new challenge for chemical physics," *Pure and Applied Chemistry*, vol. 80, no. 10, pp. 2079-2089, 2008.

[56] P. Dhamodharan, C. Manoharan, S. Dhanapandian, M. Bououdina, and S. Ramalingam, "Preparation and characterization of spray deposited Sn-doped ZnO thin films onto ITO subtracts as photoanode in dye sensitized solar cell," *Journal of Materials Science: Materials in Electronics*, vol. 26, no. 7, pp. 4830-4839, 2015.

[57] B. Choudhury and A. Choudhury, "Oxygen defect dependent variation of band gap, Urbach energy and luminescence property of anatase, anatase–rutile mixed phase and of rutile phases of TiO2 nanoparticles," *Physica E: Low-Dimensional Systems and Nanostructures*, vol. 56, pp. 364-371, 2014.

[58] F. Labat, P. Baranek, C. Domain, C. Minot, and C. Adamo, "Density functional theory analysis of the structural and electronic properties of Ti O 2 rutile and anatase polytypes: Performances of different exchange-correlation functionals," *The Journal of chemical physics*, vol. 126, no. 15, p. 154703, 2007.

[59] K. Boubaker, "A physical explanation to the controversial Urbach tailing universality," *The European Physical Journal Plus*, vol. 126, no. 1, p. 10, 2011.

[60] B. Choudhury, B. Borah, and A. Choudhury, "Extending photocatalytic activity of TiO2 nanoparticles to visible region of illumination by doping of cerium," *Photochemistry and photobiology*, vol. 88, no. 2, pp. 257-264, 2012.

[61] S. Hasegawa and F. Grey, "Electronic transport at semiconductor surfaces—from point-contact transistor to micro-four-point probes," *Surface Science*, vol. 500, no. 1-3, pp. 84-104, 2002.

[62] H.-L. Chen, Y.-M. Lu, and W.-S. J. M. t. Hwang, "Effect of film thickness on structural and electrical properties of sputter-deposited nickel oxide films," vol. 46, no. 4, pp. 872-879, 2005.

[63] B. J. R. Cullity, USA, "Elements of X-ray Diffraction. Addison and Wesley Publishing Company Inc," pp. 32-106, 1978.

[64] A. Riad, S. Mahmoud, and A. J. P. B. C. M. Ibrahim, "Structural and DC electrical investigations of ZnO thin films prepared by spray pyrolysis technique," vol. 296, no. 4, pp. 319-325, 2001.

[65] M. Mekhnache *et al.*, "Properties of ZnO thin films deposited on (glass, ITO and ZnO: Al) substrates," vol. 49, no. 5, pp. 510-518, 2011.

[66] D. P. Padiyan, A. Marikani, K. J. M. C. Murali, and Physics, "Influence of thickness and substrate temperature on electrical and photoelectrical properties of vacuum-deposited CdSe thin films," vol. 78, no. 1, pp. 51-58, 2003.

[67] H. Casey Jr, D. Sell, and K. J. J. o. A. P. Wecht, "Concentration dependence of the absorption coefficient for n− and p− type GaAs between 1.3 and 1.6 eV," vol. 46, no. 1, pp. 250-257, 1975.

[68] R. Y. Mohammed, S. Abduol, A. M. J. I. L. o. C. Mousa, Physics, and Astronomy, "Correlation between optical and structural properties of chemically deposited cds thin films," vol. 11, pp. 146-158, 2014.

[69] J. Tian, H. Deng, L. Sun, H. Kong, P. Yang, and J. J. T. S. F. Chu, "Effects of Co doping on structure and optical properties of TiO2 thin films prepared by sol–gel method," vol. 520, no. 16, pp. 5179-5183, 2012.

[70] J. Tauc, R. Grigorovici, and A. J. p. s. s. Vancu, "Optical properties and electronic structure of amorphous germanium," vol. 15, no. 2, pp. 627-637, 1966.

[71] J. Desai, S.-K. Min, K.-D. Jung, and O.-S. J. A. S. S. Joo, "Spray pyrolytic synthesis of large area NiOx thin films from aqueous nickel acetate solutions," vol. 253, no. 4, pp. 1781-1786, 2006.

[72] H. A. Juybari, M.-M. Bagheri-Mohagheghi, M. J. J. o. a. Shokooh-Saremi, and compounds, "Nickel–lithium oxide alloy transparent conducting films deposited by spray pyrolysis technique," vol. 509, no. 6, pp. 2770-2775, 2011.

[73] F. J. P. R. Urbach, "The long-wavelength edge of photographic sensitivity and of the electronic absorption of solids," vol. 92, no. 5, p. 1324, 1953.

[74] P. Mohanty, C. Rath, P. Mallick, R. Biswal, and N. J. P. B. C. M. Mishra, "UV–visible studies of nickel oxide thin film grown by thermal oxidation of nickel," vol. 405, no. 12, pp. 2711-2714, 2010.

[75] S. Nandy, B. Saha, M. K. Mitra, and K. J. J. o. m. s. Chattopadhyay, "Effect of oxygen partial pressure on the electrical and optical properties of highly (200) oriented p-type Ni 1− x O films by DC sputtering," vol. 42, no. 14, pp. 5766-5772, 2007.

Abstract

Abstract:

this work is concern the study of the structural, optical and electrical characteristics of thin -films of pure nickel oxide (NiO), and cobalt (Co) doped (NiO) using (0, 1 ,3 ,5) % concentrations, where the deposition of thin-films is realized on glass substrates under temperature ($400C^{\circ}$) by spray pyrolysis technique, X- ray diffraction results have shown that the thin films prepared have a cubic crystalline structure. The main characteristic peaks are assigned to the (111) and (200) planes. The transmittance of Co doped nickel oxide thin films increases rapidly as the wavelength increases in the range of (300 - 350) nm. The band gap values decreases when the Co concentration increases and these values are between 3.49 eV and 3.65 eV. Urbach's energy increases with the concentration of Co, and the perfect film doped conductivity is obtained for the percentages 1%.

Keywords: Spray Pyrolysis Technique (SPT); NiO Thin Films; Transparent Conductive Oxides (TCO); Cobalt.

Résumé:

Le travail concerne l'étude des caractéristiques structurelles, optiques et électriques de films minces d'oxyde de nickel pur (NiO) et de (NiO) dopé cobalt (Co) à des concentrations de (0, 1,3,5) %, où le dépôt de -les films sont réalisés sur des substrats de verre sous température (400 C °) par technique de pyrolyse par pulvérisation, les résultats de diffraction des rayons X ont montré que les films minces préparés ont une structure cristalline cubique. Les principaux pics caractéristiques sont affectés aux plans (111) et (200). La transmittance des films minces d'oxyde de nickel dopés au Co augmente rapidement lorsque la longueur d'onde augmente dans la plage de (300 à 350) nm. Les valeurs de la bande interdite diminuent lorsque la concentration de Co augmente et ces valeurs sont comprises entre 3,49 eV et 3,65 eV. L'énergie d'Urbach augmente avec la concentration de Co, et la conductivité dopée du film parfait est obtenue pour les pourcentages de 1%.

Mots clés: Technique de spray pyrolyse (SPT); couches minces NiO; Oxydes conducteurs transparents (TCO); Cobalt.

ملخص :

يهتم هذا العمل بدراسة الخصائص التركيبية والبصرية والكهربائية للأغشية الرقيقة لأكسيد النيكل النقي (NiO) ، والنيكل المخدر بالكوبالت (Co) باستخدام تركيزات (0،1،3،5)٪ ، حيث ترسب طبقة رقيقة. - يتم تحقيق الأغشية على ركائز زجاجية تحت درجة حرارة (400 درجة مئوية) بتقنية الانحلال الحراري بالرش ، وقد أظهرت نتائج حيود الأشعة السينية أن الأغشية الرقيقة المحضرة لها بنية بلورية مكعبة. يتم تعيين القمم المميزة الرئيسية للطائرات (111) و (200). تزداد نفاذية الأغشية الرقيقة لأكسيد النيكل المشوب بالكربون بسرعة مع زيادة الطول الموجي في نطاق (300 -350) نانومتر. تنخفض قيم فجوة النطاق عندما يزيد تركيز Co وتتراوح هذه القيم بين 3.49 فولت و 3.65 فولت. تزداد طاقة طاقة اورباخ مع تركيز Co ، ويتم الحصول على الموصلية المثالية للغشاء المشبع بالنسبة المئوية 1٪.

الكلمات المفتاحية : تقنية الانحلال الحراري بالرش (SPT) ؛ أفلام رقيقة NiO ؛ أكاسيد موصلة شفافة (TCO) ؛ كوبالت.